LASER/OPTICS TECHNIQUES 2ND INTERIM SUMMARY REPORT

Prepared For: National Aeronautics and Space Administration,
George C. Marshall Space Flight Center, Huntsville, Alabama

PERKIN-ELMER

PERKIN-ELMER

OPTICAL GROUP, NORWALK, CONNECTICUT

ENGINEERING REPORT NO. 8631

LASER/OPTICS TECHNIQUES

2ND INTERIM SUMMARY REPORT

DATE: 31 DECEMBER, 1966

PREPARED FOR: GEORGE C. MARSHALL SPACE FLIGHT CENTER

NATIONAL AERONAUTICS AND SPACE ADMINISTRATION

HUNTSVILLE, ALABAMA

CONTRACT NO. NAS 8-20115

Prepared by: Morley S. Lipsett

Morley S. Lipsett, Senior Physicist

Approved by: H.F. Wischnia

H.F. Wischnia, Senior Staff Engineer

SPO 26872

Contributors

M. S. Lipsett, Project Manager

E. R. Schlesinger

S. R. Habijanec

R. C. Liu

W. A. Roman

R. A. Arnold

TABLE OF CONTENTS

LIST OF ILLUSTRATIONS

LIST OF ILLUSTRATIONS (Continued)

LIST OF ILLUSTRATIONS (Continued)

ABSTRACT

The development of transmit beam offset and coarse acquisition equipment for the Laser/Optics Techniques breadboard is described. In addition, preliminary acquisition and track simulation experiments carried out in the laboratory with the breadboard hardware are described.

SECTION I

SUMMARY

This report describes work carried out for MSFC which extends the development of key hardware for a deep-space optical communications system. In particular, a transmit beam offset subsystem and a coarse acquisition subsystem have now been added to the Laser/Optics Techniques breadboard[1] (termed the "laser telescope" in this report). In addition, preliminary acquisition and track simulation experiments have been carried out in the laboratory with the breadboard hardware.

It was originally planned that the transmit beam offset subsystem would have the sole function of implementing the transmitter point-ahead function required for Bradley effect compensation. Subsequently, it developed that the same servo-controlled pair of Risley prisms recommended for this purpose could also be employed as a means for vehicle-roll compensation. Indeed, analysis revealed that this additional function could be carried out comparatively easily. A roll-compensation capability was, therefore, designed into the transmit beam offset subsystem and is now incorporated as part of the breadboard. As a result the overall design of the laser telescope has been decisively simplified.

Optical wedges were used with a maximum net offset (referred to the output of the telescope) of 6 arc-seconds, which corresponds to synchronous orbit requirements. It was found that the magnitude of the offset could be

[1]Perkin-Elmer Engineering Report No. 8387 (Laser/Optics Techniques, First Interim Summary Report).

remotely adjusted to better than 1/10 arc-second peak error. Similarly, it was found that the rotational coordinate about the line of sight could be remotely adjusted to an accuracy appreciably better than needed to maintain diffraction-limited pointing precision. Moreover, this accuracy was found to be maintained over a full 360 degrees of roll about the line of sight. Thus, within the bandwidth of the servos, which is such that a roll error of less than 1 arc-minute results for a roll rate of 1/2 degree per second, compensation for spacecraft roll is adequately provided for by this subsystem.

Although operating parameters for the transmit beam offset subsystem were chosen on the basis of the accuracy requirements of a Laser Communications Satellite Experiment (LCSE) at a synchronous orbit, the design is straightforwardly adaptable to future deep-space applications.

Basic simplicity and reliability were the characteristics emphasized in the development of the coarse acquisition subsystem for the breadboard. The subsystem employs a precision optical element that functions as a combination field lens/field splitter. This element divides the 1-degree coarse acquisition field into four segments and directs the light beam from each quadrant onto a small circular patch in the respective quadrant in the plane of a suitable detector. In the present case, an EMR quadrant multiplier phototube is used as the detector. It functions as would four distinct photomultipliers with a mechanical chopper, but accomplishes the same thing with four photocathodes and a common dynode chain - all contained in a small package - with the aid of electronic switching circuitry.

The transmit beam offset and coarse acquisition subsystems are identified in the schematic layout of the entire laser telescope shown in Figure 1-1 and in the photograph of the breadboard apparatus shown in Figure 1-2.

Laboratory experiments were carried out to demonstrate beacon acquisition and precision pointing and tracking under conditions that simulate space operation of the laser telescope. The intent was first to provide a visual display of the fractional arc-second ($\sim$ 1/10 arc-second) tracking accuracy of the breadboard and, second, to investigate the suitability of the equipment for future extensive experiments to simulate acquisition, tracking, and pointing accuracies of an LCSE spacecraft.

In the light of this most recent phase of the Laser/Optics Techniques Program, it is recommended that future work proceed along the following directions:

1) Modify the system to use a CO_2 laser transmitter (for operation at 10.6 microns) in addition to the helium-neon laser transmitter currently being used.

2) Perform dynamic laboratory space simulation of acquisition tracking and pointing maneuvers, including "station transfer" with the Laser/Optics Techniques breadboard apparatus.

The outcome that we may expect from such future work is another step in demonstrating the feasibility of key hardware that can be called upon in the future for use in a deep-space optical communication system.

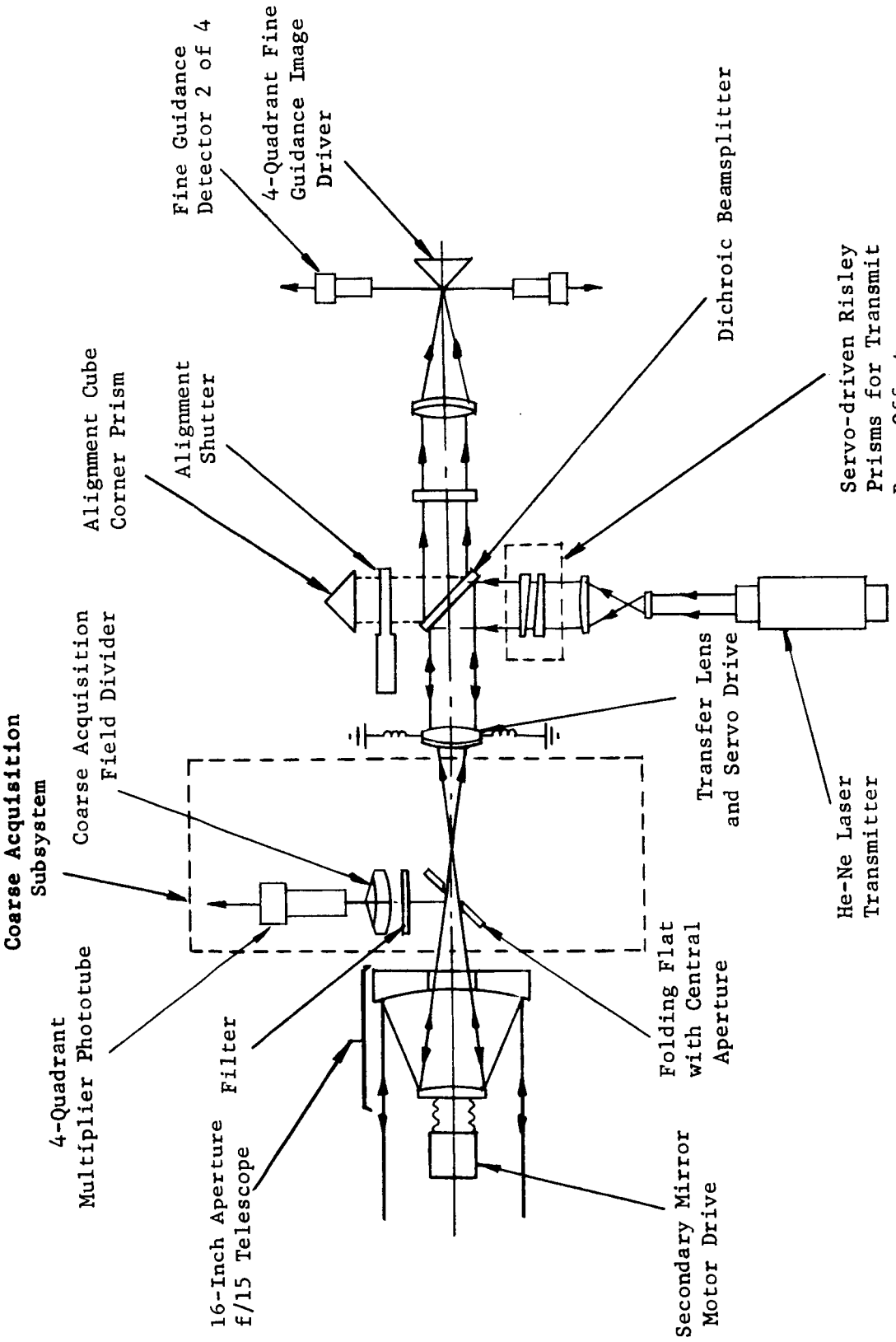

Figure 1-1. Layout of Breadboard Equipment

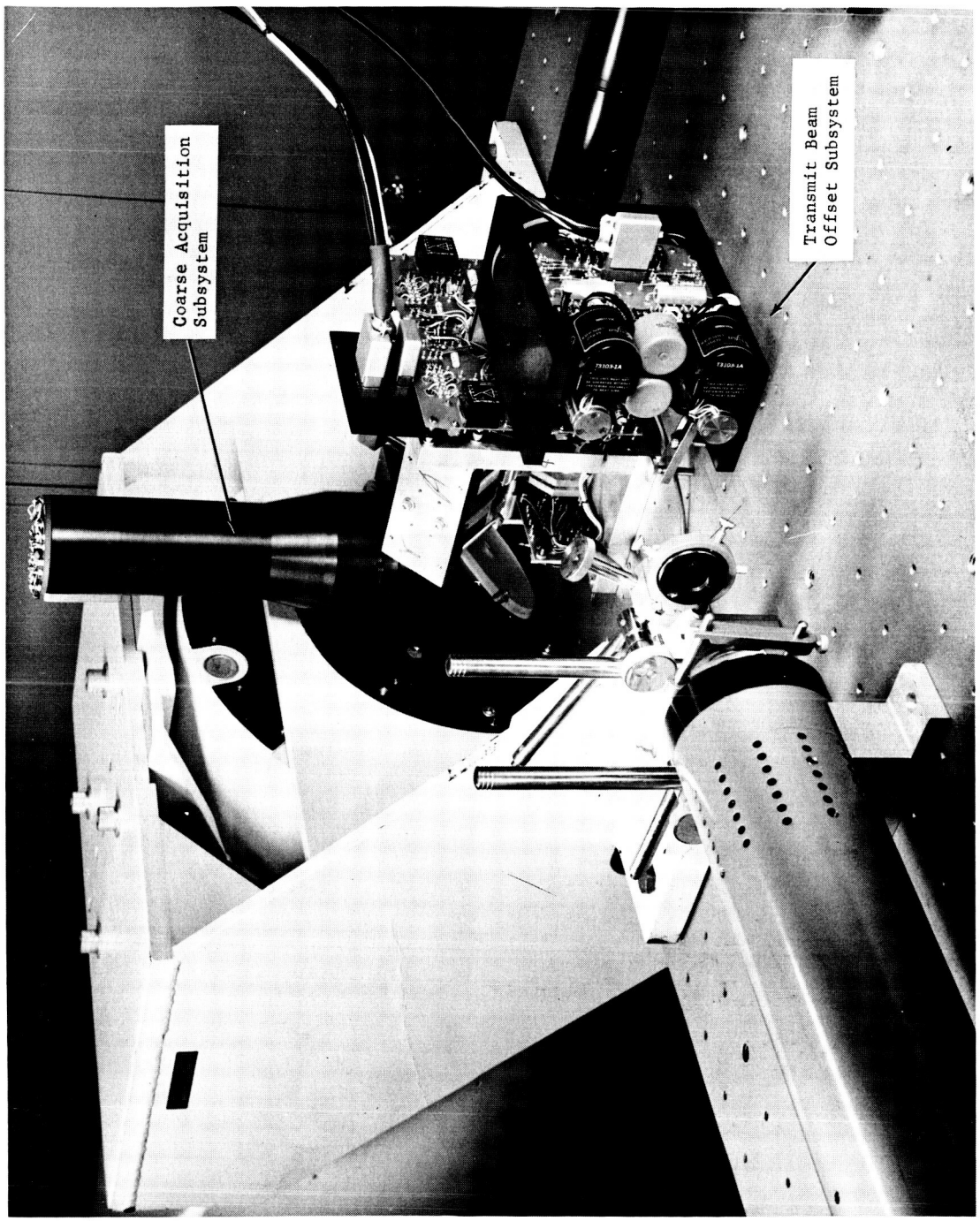

Figure 1-2. Photograph of the Breadboard Apparatus

SECTION II

TRANSMIT BEAM OFFSET SUBSYSTEM

2.1 GENERAL CONSIDERATIONS

A diffraction-limited optical communication telescope must be aimed extremely precisely. From a reception standpoint, pointing errors about the line of sight should be limited so that the field-of-view requirements are minimized. From the transmission standpoint, a pointing error exceeding half the telescope resolution ($\approx 0.61\ \lambda/D$) appears to a distant receiver as an appreciable reduction in transmitted power. Defining $0.61\ \lambda/D$ as the "allowed pointing error", we note that this constraint is stringent and, for example, requires error limits of ±1/2 arc-second peak for a relatively small aperture system (5-inch diameter) operating in the visible (Figure 2-1).

In general there will always exist a finite relative transverse velocity, v, between a spaceborne laser telescope and its associated ground station. Because of this, the apparent beacon line of sight as seen by the spacecraft will differ from the correct aiming direction if the transmitted beam is to hit the ground station at or near the beacon (Figure 2-2). Assuming initial boresight alignment of the transmit and receive lines of sight by the techniques discussed in reference 1,* the magnitude of the offset angle, θ, away from this boresight reference is given simply by $\theta = \frac{2v}{c}$, where c is the velocity of light.

---

* Op.cit., page 1-1

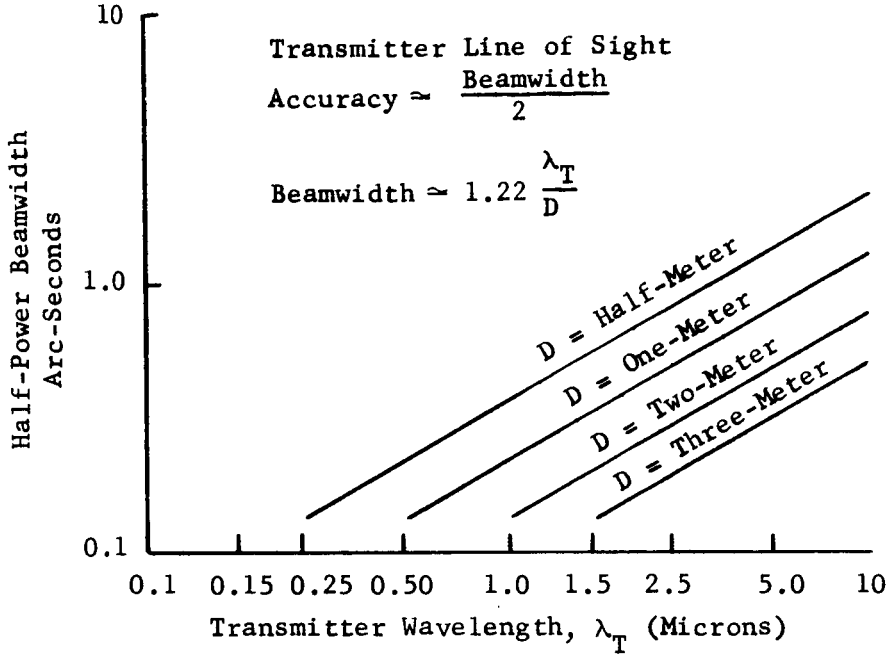

Figure 2-1. Pointing Requirements

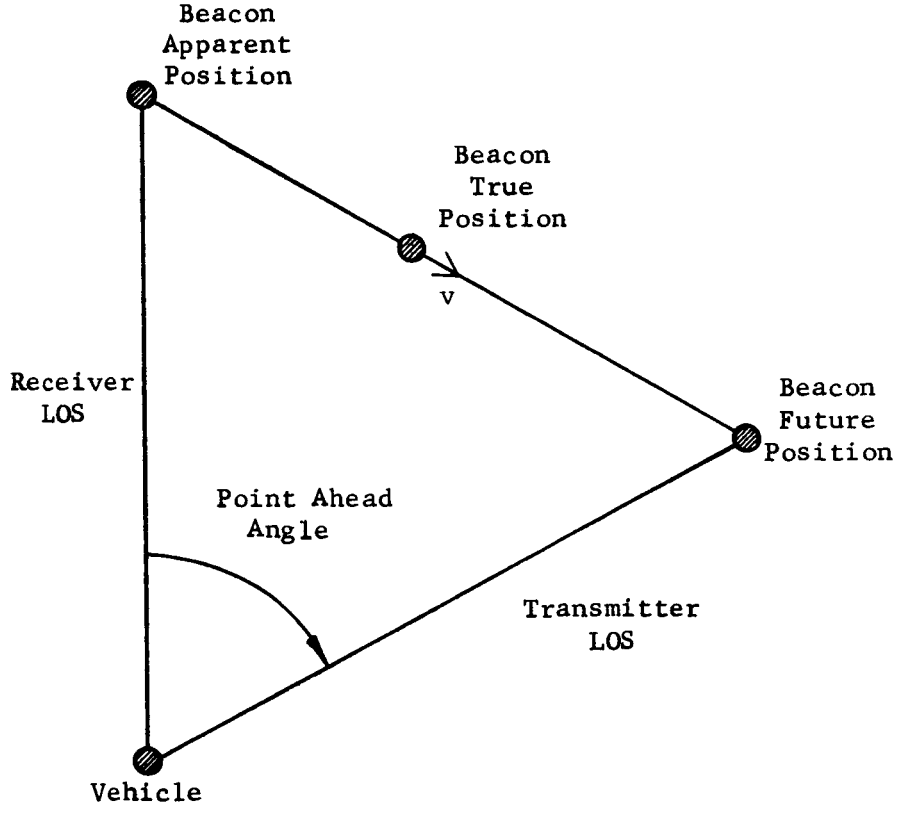

Figure 2-2. Example of Point Ahead

For the case of a 16-inch aperture, 6328Å telescope at synchronous altitude and in communication with an earth station, the point-ahead angle ($\approx$ 4 arc-seconds) so greatly exceeds the telescope's half resolution (0.2 arc-seconds) that some means of controlled point ahead is required. The situation is even worse for a Martian probe where angular differences of up to 36 arc-seconds can be anticipated.

2.1.1 Accuracy Requirements

For the synchronous orbit application as shown in Figures 2-3 and 2-4, the magnitude and direction* of the point-ahead angle must be implemented with accuracies of about

$$M_{PA} = 0.707\ (0.2 \text{ arc-second}) \approx 0.14 \text{ arc-second}$$
(or 3.5 percent of 4 arc-seconds)

and

$$\Delta\theta_{PA} = \frac{0.707\ (0.2 \text{ arc-second})}{4 \text{ arc-seconds}} \approx 2 \text{ degrees}$$

respectively, while the corresponding Martian probe requirements are approximately 0.14 arc-second (or 0.39 percent of 36 arc-seconds) and 13.5 arc-minutes.

In either case, the point-ahead information is slowly varying and can be computed on the ground and transmitted to the laser telescope, which is oriented to some known rotational reference. While this is feasible, it is preferable to avoid the associated tight roll orientation requirements. This is possible if the roll positioning is sensed and used to correct the point-ahead direction data as received from earth. [It should be noted that this correction should not be made at the earth station (in order to avoid on-board

*i.e., Rotational orientation about the line of sight.

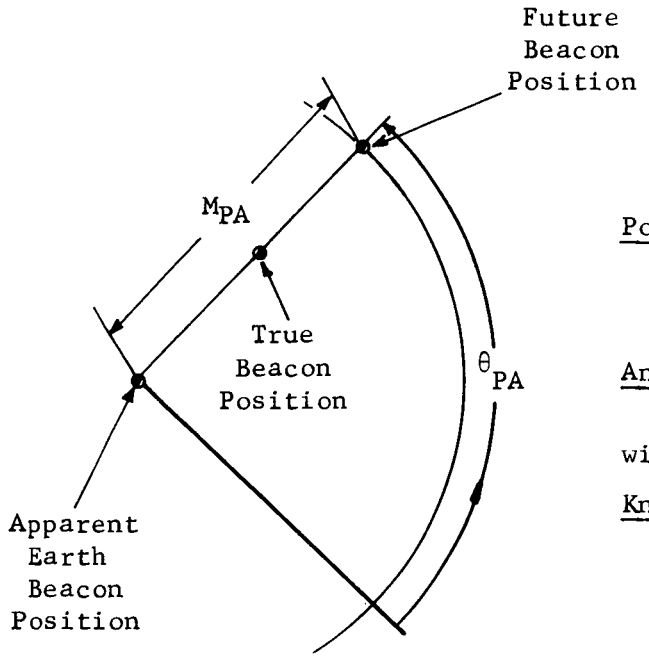

REQUIRED DATA:

Point Ahead Magnitude (M_{PA})

and

Angle Information (θ_{PA})

with respect to a

Known Reference Direction

Figure 2-3. Point-Ahead Geometry

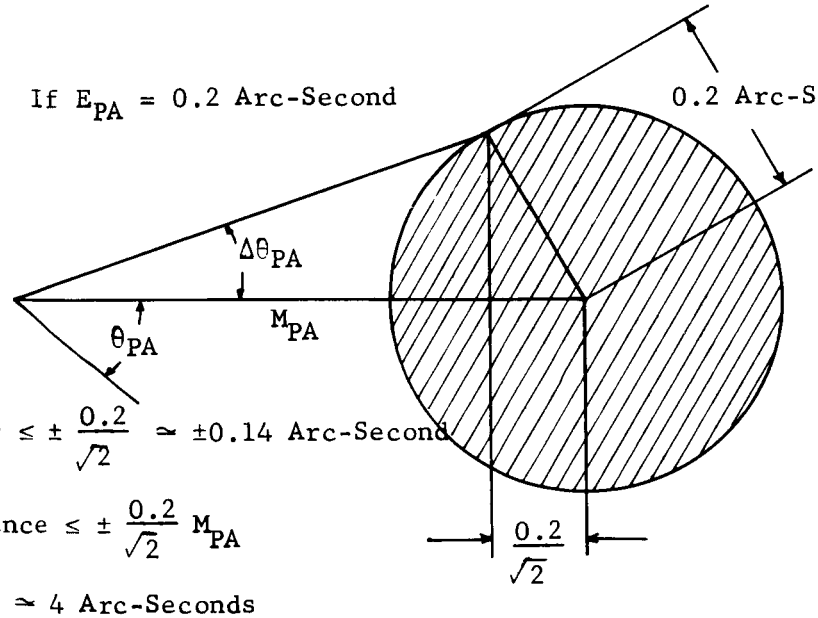

then M_{PA} Error $\leq \pm \frac{0.2}{\sqrt{2}} \simeq \pm 0.14$ Arc-Second

and θ_{PA} Tolerance $\leq \pm \frac{0.2}{\sqrt{2}} M_{PA}$

$= 2.0° \big|_{M_{PA}} \simeq 4$ Arc-Seconds

Note: $\frac{0.2}{\sqrt{2}x4} \simeq 3.5\%$

Figure 2-4. Point-Ahead Accuracy

equipment) since the communication round-trip transit time is comparable to, or greater than, expected roll error component periods.]

2.1.2 Implementation

A suitable implementation for transmit beam offset and roll compensation incorporates Risley prism optical elements for transmit beam control and a solar tracker for roll error sensing as depicted in Figures 2-5 and 2-6. In operation, the telescope is nominally oriented to a known attitude (or coordinate system) so that two commands computed on the ground can correctly control the separate Risley positions and, so, properly direct the transmitter line of sight (LOS).

The attitude of the telescope would be with its receiver LOS directed towards the ground station and, in this case, a roll orientation directing its roll error sensor at the sun. (See Figure 2-7.) The sun tracker has a gimbal normal to the receiver LOS for accommodating varying "sun - earth-station" angles plus an axis, θ_c, parallel to the LOS.

The gimballing servo control arrangement is such that θ_c will stay at a zero position if the telescope is correctly roll oriented. Errors in roll orientation, on the other hand, cause counter rotations of the θ_c axis, which can therefore be used to introduce compensating motions into both Risley control servos in the manner indicated.

The transmit beam offset subsystem as described consists of a two-axis servo-controlled gimballed star tracker, two digital-input-command

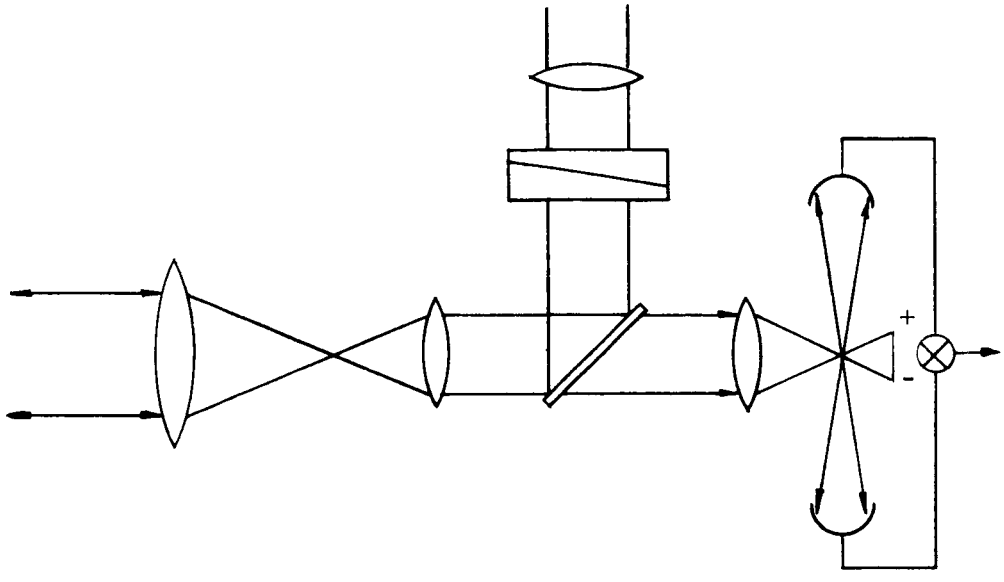

Aligned Condition

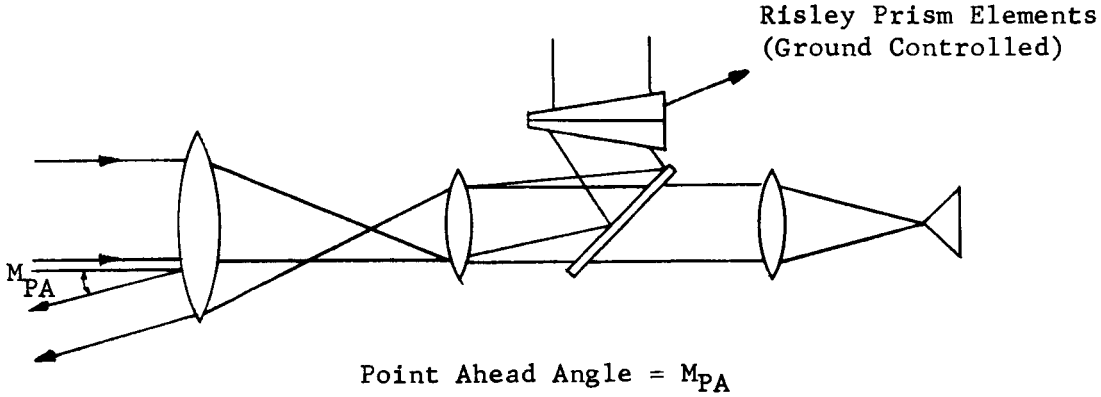

Point Ahead Angle = M_{PA}

Point Ahead Condition

Figure 2-5. Typical Common Optics Telescope Arrangement

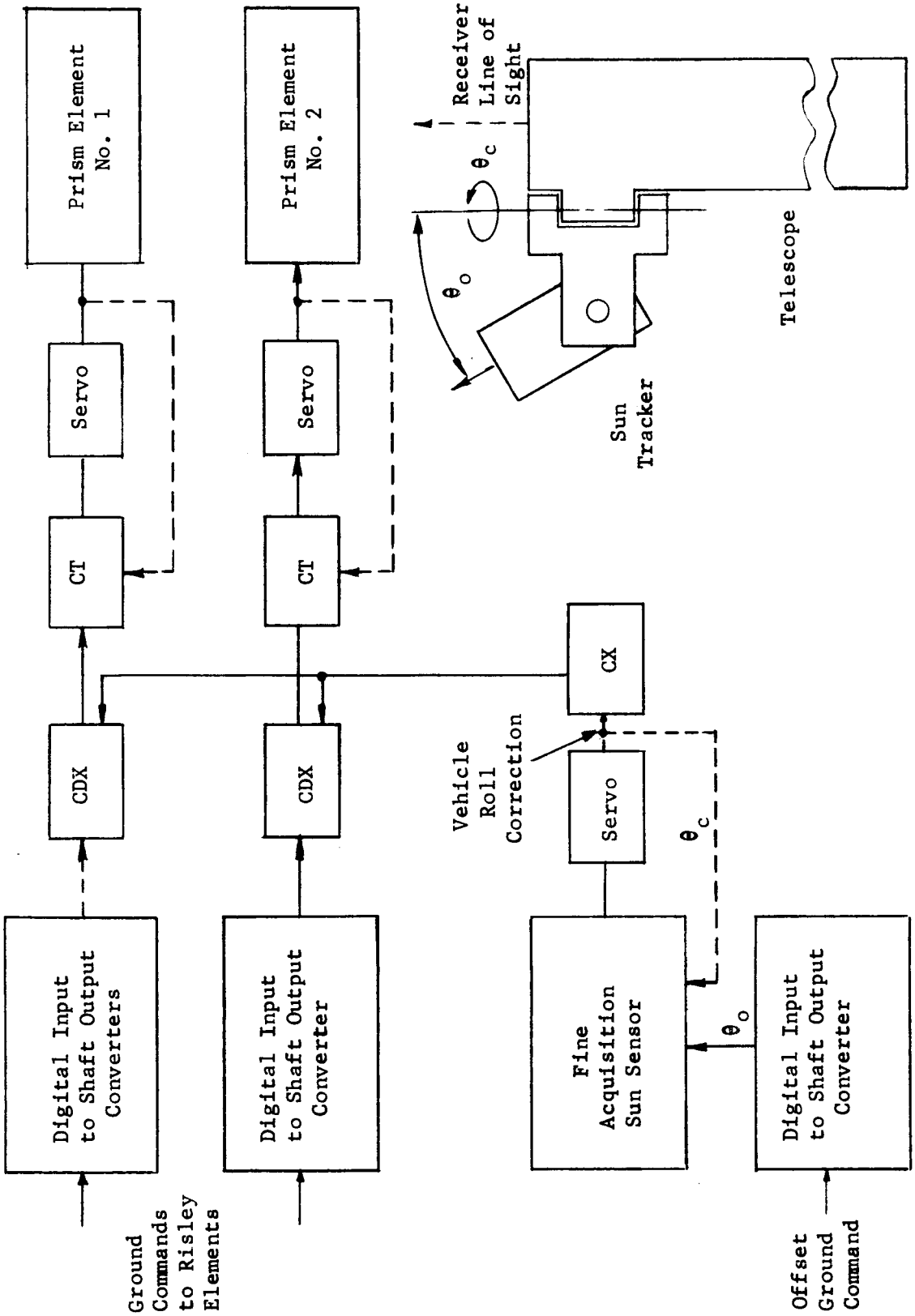

Figure 2-6. Typical Mechanization of Point Ahead

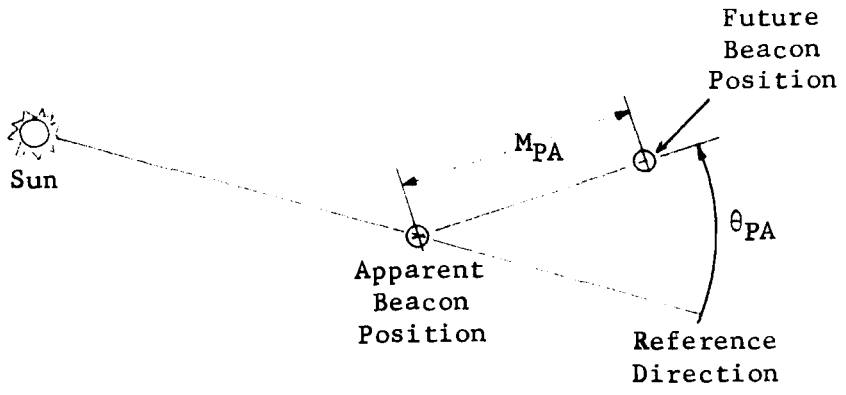

Figure 2-7. Roll Reference Direction Supplied by the Sun

to-shaft-angle converters, and two synchro type servo systems which control the angular positions of two Risley prism elements.

The transmit beam offset subsystem constructed for the special requirements of the Laser/Optics Techniques Program consists of two synchro-type servos, plus three goniometers which manually simulate the synchro shaft inputs normally provided by the sun tracker (θ_c) and two digital-input-to-shaft-angle converters.

This hardware, which consists of a rack-mounted subassembly (Figure 2-8) and an optical subassembly (Figure 2-9), was designed to meet the accuracy requirements stated previously for the 16-inch communicator in synchronous orbit, higher accuracies being considered as desirable and straightforwardly attainable but not necessary to demonstrate approach feasibility.

2.2 TECHNICAL DISCUSSION OF TRANSMIT BEAM OFFSET SUBSYSTEM

2.2.1 Accuracy

The precision of transmit line-of-sight offset control attained by the equipment can be predicted from a consideration of Risley prism action

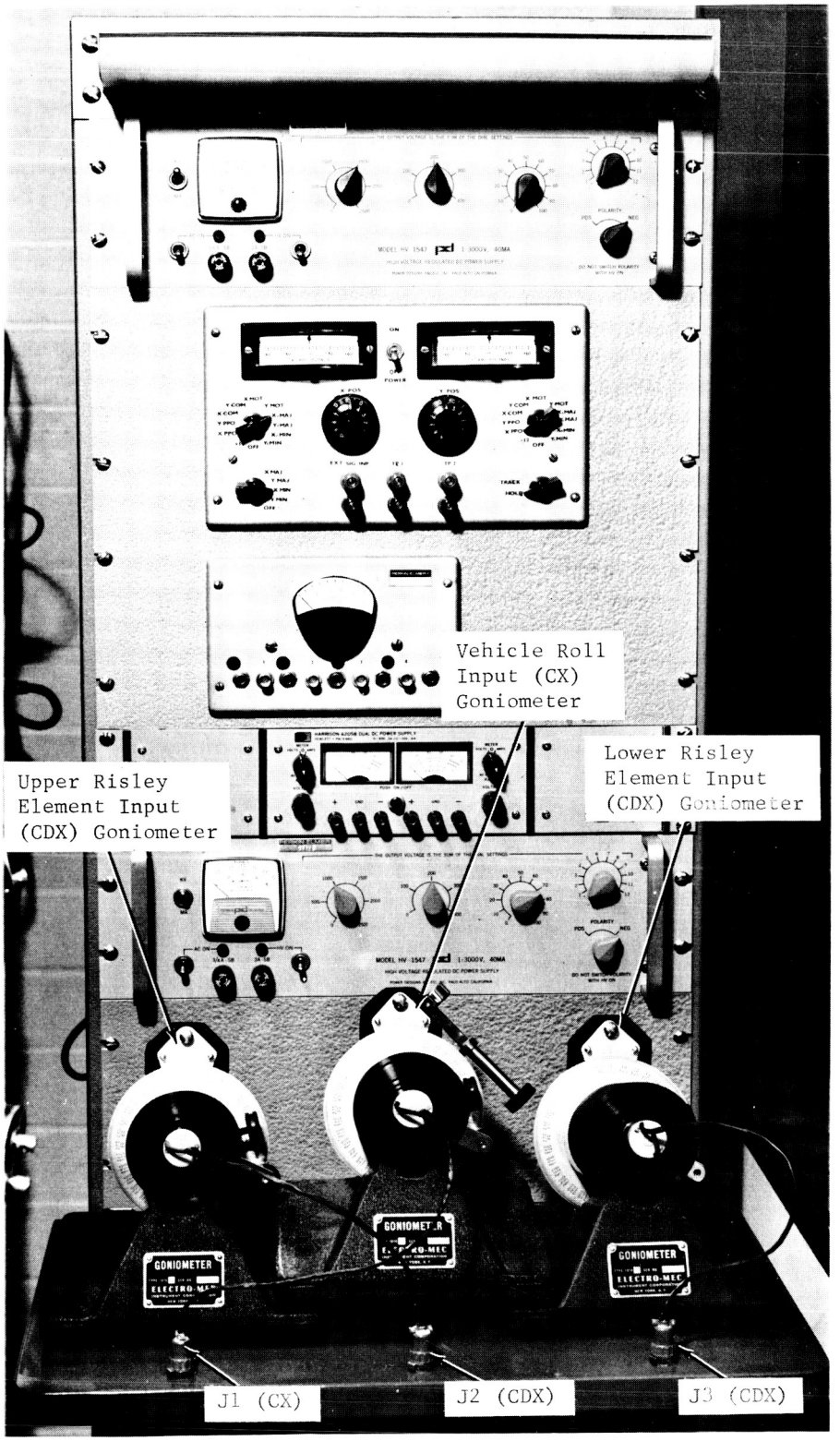

Figure 2-8. Rack-Mounted Equipment (Front View)

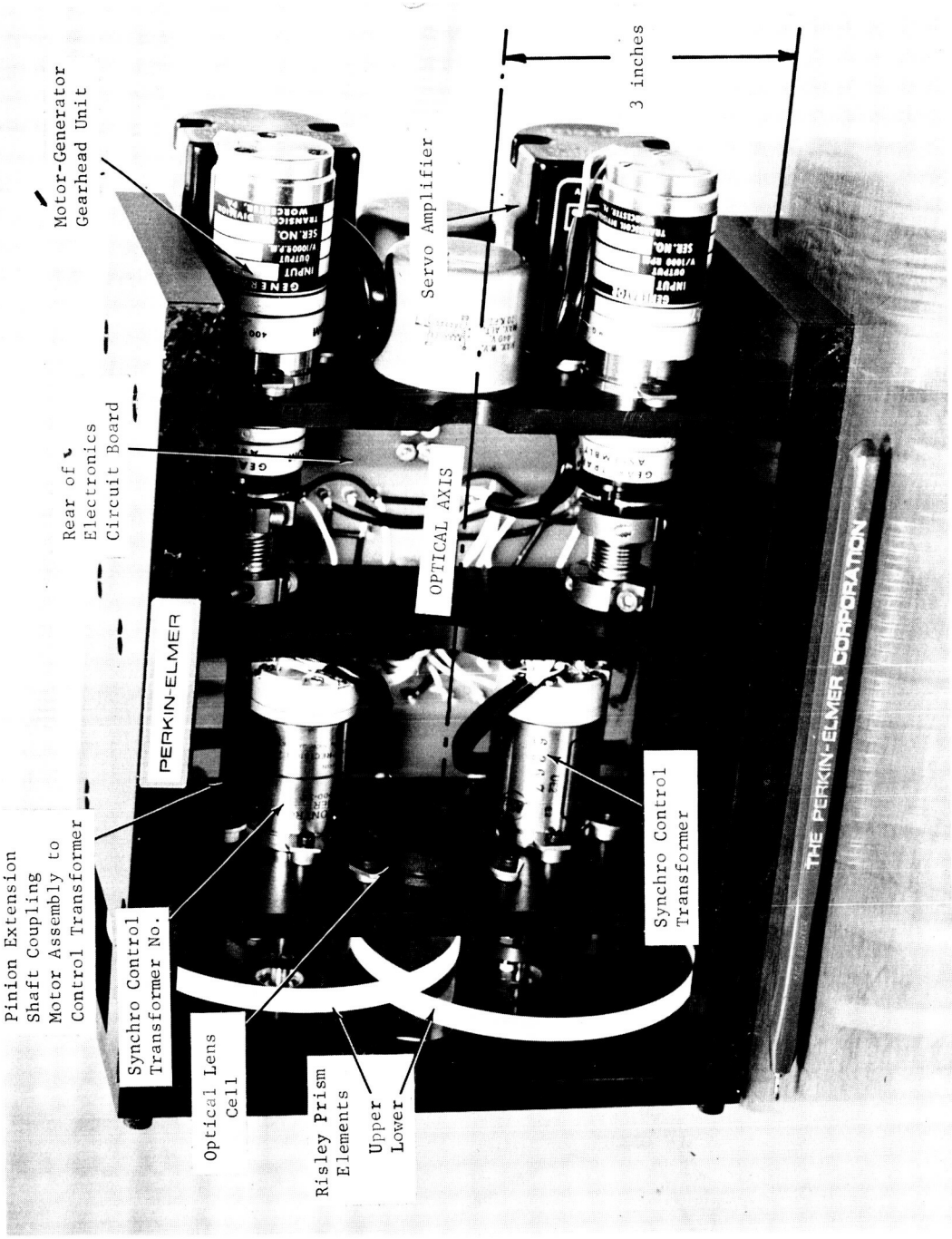

Figure 2-9. Transmit Beam Offset Subsystem and Mechanical Subassembly

and element positioning accuracy. The equation relating prism induced deviation δ' to element apical angle $\alpha_1=\alpha_2=\alpha$ and relative angular position β is

$$\delta' = (n-1)\ 2\alpha \sin\frac{\beta}{2} \approx \alpha \sin\frac{\beta}{2}$$

where β is taken to be zero for the condition of zero net prism induced deviation.

The two Risley elements, however, deviate collimated transmitter light in the optical system where their combined 10-arc-minute deviation produces a 6-arc-second line-of-sight deviation referred to telescope object space. The expression for Risley induced LOS deviations can thus be expressed as

$$\delta = 6 \sin\frac{\beta}{2} \text{ arc-seconds} \approx M_{PA}$$

Let us now consider this expression in light of the expected Risley servo errors as tabulated in Table 2-1.

If the two Risley prisms have equal angular errors, θ_ϵ, then the magnitude of transmit beam offset, M_{PA}, will be correct while the direction of offset θ_{PA}, will be in error, $\Delta\theta_{PA}$, by θ_ϵ. If the two prisms, however, have angular error θ_ϵ differing only in sign, then θ_{PA} will be correct but M_{PA} will be in error, i.e.:

$$\Delta M_{PA} = \Delta\beta \frac{d\delta}{d\beta} = 6\Delta\beta d \frac{\sin \beta/2}{d\beta} = 6 \frac{\Delta\beta}{2} \cos\frac{\beta}{2} = 6\theta_\epsilon \cos\frac{\beta}{2} \text{ arc-seconds}$$

since $\Delta\beta = 2\theta_\epsilon$

TABLE 2-1. EXPECTED RISLEY SERVO ERRORS

Source	Maximum Magnitude (Arc-Minutes)
Goniometer (CX) *	6
Synchro Transmitter, CX	7
Goniometer (CDX) *	6
Synchro Differential, CDX	7
Servo Static Accuracy	4
Synchro Transformer, CT	7
Sum of Absolute Errors	37
RMS Error	15.3

* The goniometer can, by means of a vernier, be read to 1 arc-minute and the graduation accuracy is ±15 arc-seconds. The anticipated ± 1-1/4 arc-minute error was increased to 6 arc-minutes to more realistically approximate the errors which might be associated with the digital-input-command-to-shaft-angle converters and the star tracker inputs.

Hence, the 37-arc-minute absolute maximum error could produce either a maximum ΔM_{PA} of $6 \frac{37}{60x57.3} \cos\theta = 0.0646$ arc-second, or a maximum $\Delta\theta_{PA} = 37$ arc-minutes. [At $M_{PA} = 4$ arc-seconds, this represents a pointing error of $M_{PA}\Delta\theta_{PA} = (4)\left(\frac{37}{57.3x60}\right) = 0.043$ arc-second.]

The RMS pointing errors expected are $\Delta M_{PA} = 0.027$ and $M_{PA}\Delta\theta_{PA} = 0.018$ arc-second. It is noteworthy that, for this application, the absolute maximum static errors are within the allowed error by a significant safety factor (>3).

This means that a reasonable fraction of allowed error can be allotted for receiver LOS (or ground beacon tracking) errors which directly degrade

transmitter LOS accuracy. (Refer to Figure 2-10.)

Dynamic error components are expected to cause negligible degradations since the servo offers a Risley element slewing speed of 3/4 revolution per second and a velocity constant* of 30.

2.2.2 Hardware Description (Refer to Figure 2-11)

The design is conventional with the synchro transformer (CT) error signal amplified by a nominal gain of 100 before being applied to the servo motors. The 6.8K ohm and the 33K ohm resistors together set the amplifier gain while the 10-volt Zener diodes prevent excessive amplifier input voltages. The 68-volt Zener diodes provide protection against possible power supply transients while the 2-microfarad capacitors tune the motor loads to near unity power factor. Velocity feedback is incorporated by connecting the CT and the tachometer winding in series. Figure 2-12 indicates the physical location of the terminal boards, connectors, test points and parts which are shown in Figure 2-11.

The mechanical arrangement features a motor-to-CT geardown of 118, being accomplished in two steps: an integral gearhead reduction of 10 followed by an external pair of gears which are spring loaded to avoid possible instabilities due to excessive backlash. Each CT and its associated prism element are directly coupled to avoid gearing errors. It should be noted that the goal in this instance was to demonstrate the feasibility of the approach. Therefore efforts to obtain minimum size, maximum accuracy, and

*Velocity Constant $\approx \frac{\text{Output Rate (degrees/second)}}{\text{Output error (degrees) to maintain the rate}}$

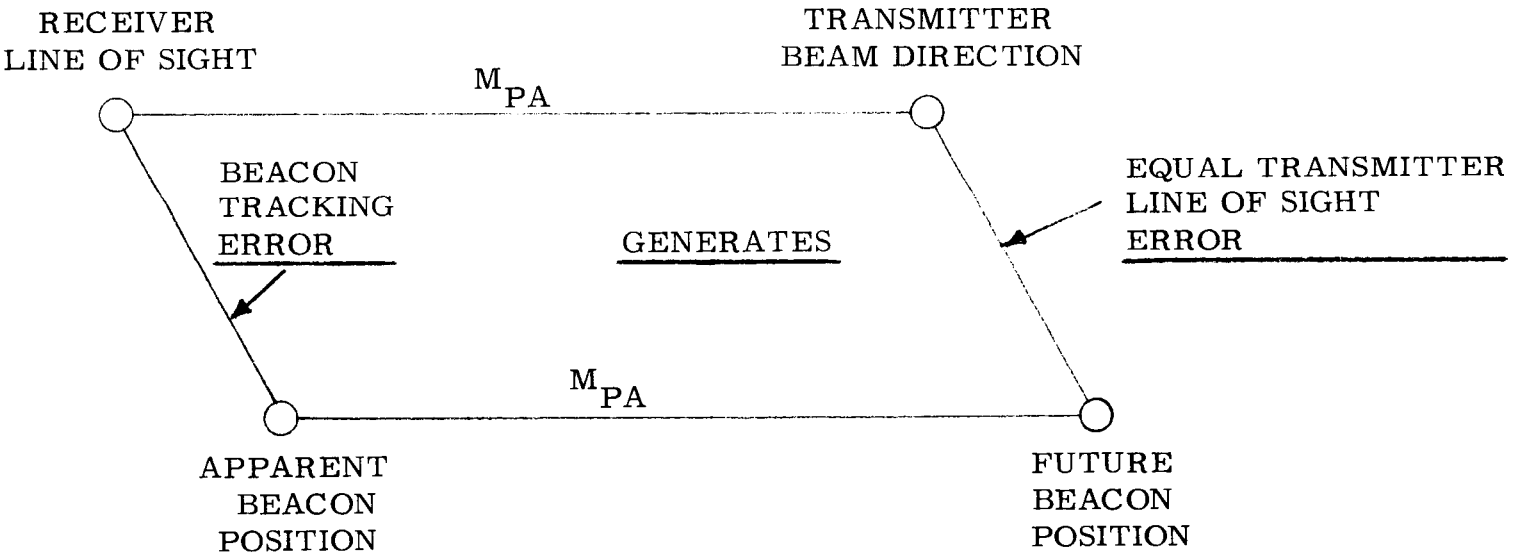

$$\left[\begin{array}{c}\text{ALLOWED}\\ \text{POINT AHEAD}\\ \text{ERROR}\end{array}\right] = \left[\frac{\text{BEAMWIDTH}}{2}\right] - \left[\begin{array}{l}\text{BEACON TRACK}\\ \text{ERROR } E_B\end{array}\right]$$

$$E_{PA}\Big|_{max} = \frac{BW}{2} - E_B$$

Figure 2-10. Illustration of Relationship Between Tracking error and Transmit LOS Error. The allowed point-ahead implementation error must be less than half the transmitter beamwidth to allow for beacon tracking errors.

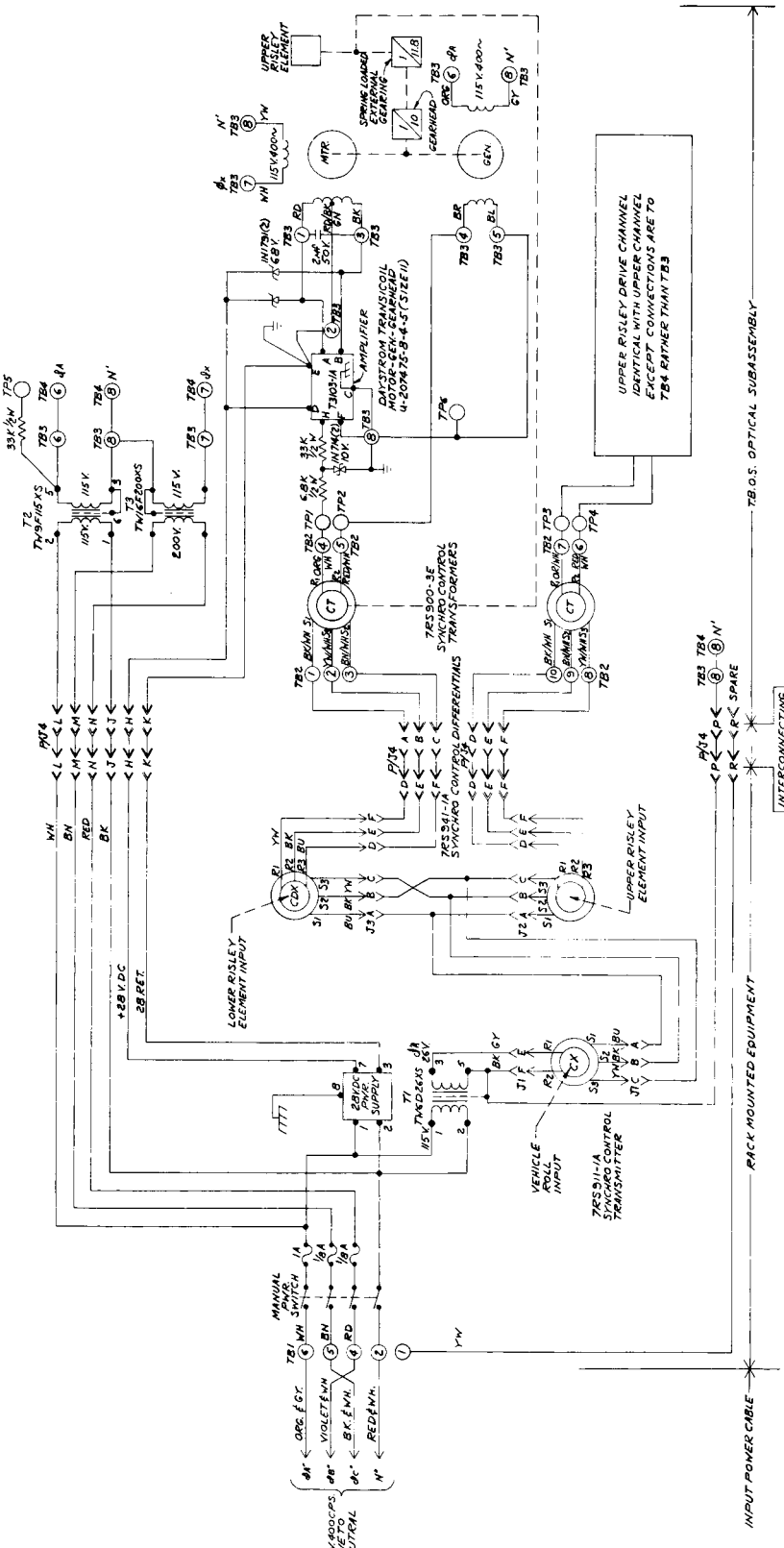

Figure 2-11. Transmit Beam Offset Subsystem, Wiring and Schematic Diagram

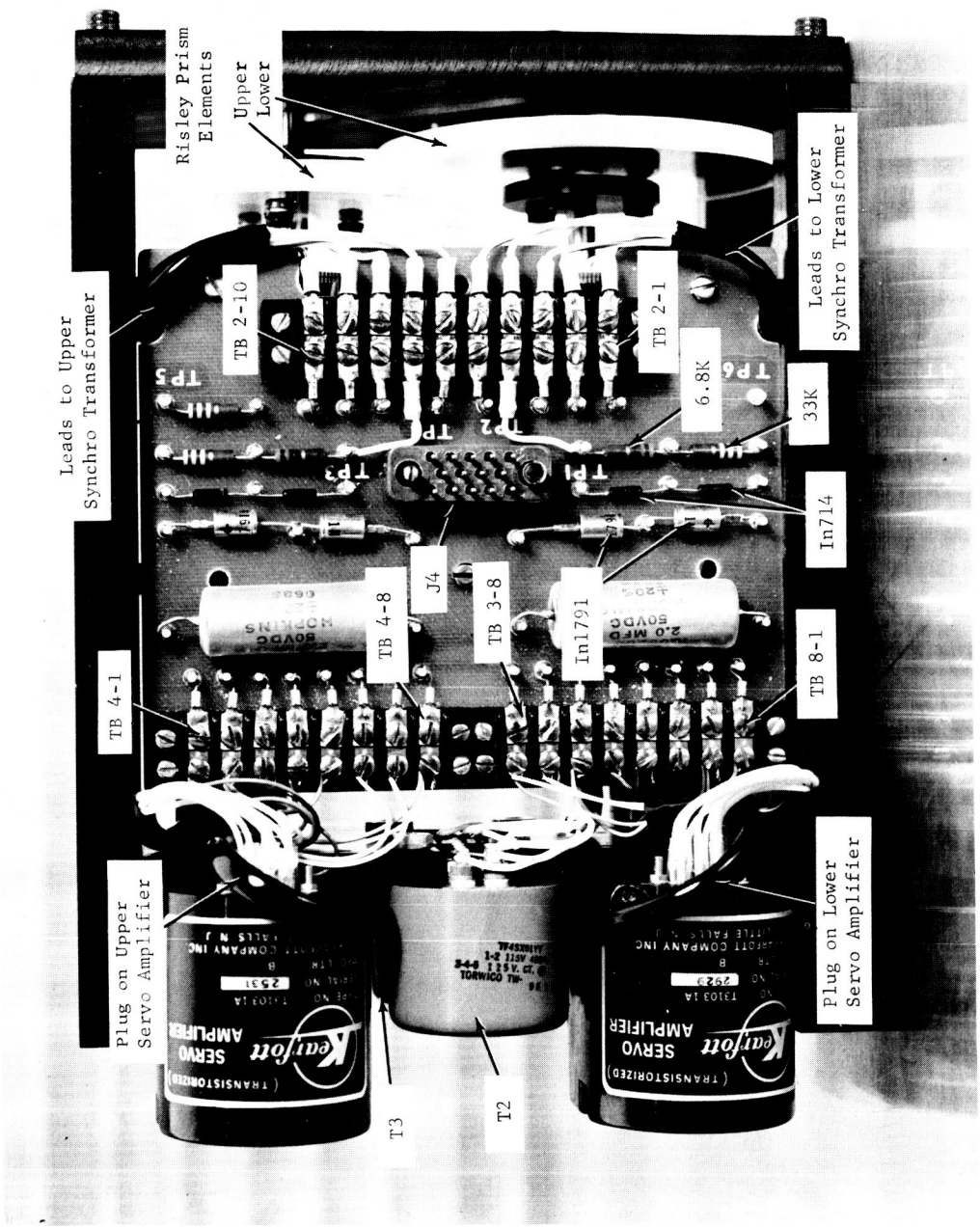

Figure 2-12. Optical and Mechanical Subassembly Circuit Board

smallest power consumption were not specifically emphasized.

The optical and mechanical subassembly shown in Figure 2-9, could be considerably miniaturized by mounting small prism elements within larger diameter, high accuracy, hollow shaft CT units driven possibly by direct drive torquer motors (or small rim driving motors).

2.2.3 Servo Design (Refer to Figure 2-13)

The nominal closed loop response (CLR) of the minor loop including the amplifier and motor-tachometer is expressible as

$$CLR\Big|_{minor} = \frac{\frac{AK_m}{JS^2 + RS}}{1 + \frac{AK_m}{JS^2+RS} K_T S} = \frac{AK_m}{JS^2 + (R+AK_m K_T)S}$$

where J is the total inertia expressed at the motor shaft. The nominal closed loop response (CLR) of the major loop is now expressible as

$$CLR\Big|_{major} = \frac{CLR\Big|_{minor} \times \frac{1}{N} \times K_p}{1 + CLR\Big|_{minor} \times \frac{1}{N} \times K_p}$$

where N is the overall geardown (118), and K_p is the CT scale factor $\left(23 \frac{\text{volts rms}}{\text{radian}}\right)$

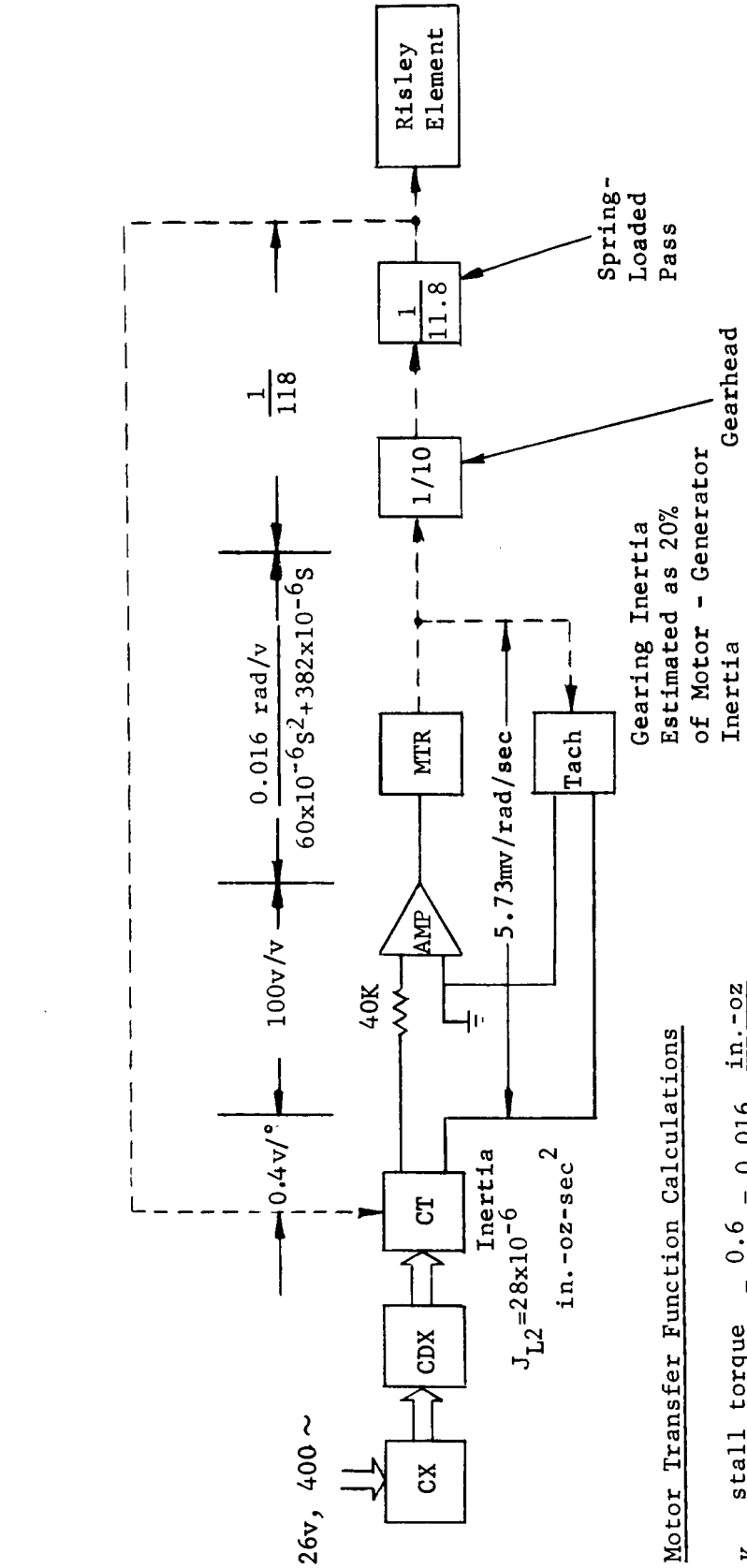

Motor Transfer Function Calculations

$$K_M = \frac{\text{stall torque}}{\text{rated voltage}} = \frac{0.6}{36} = 0.016 \ \frac{\text{in.-oz}}{\text{volt}}$$

$$R = \frac{0.4 \times \text{stall torque}}{\text{No Load Speed}} = 382\times10^{-6} \ \frac{\text{in.-oz}}{\text{rad/sec}}$$

$$J \approx 1.2 \times \text{motor-gen. inertia} + \frac{\text{load inertia}}{N^2}$$

$$\approx 1.2\times50\times10^{-6}\ \text{in.-oz-sec}^2 + \frac{0.01}{(118)^2} \approx 60 \times 10^{-6}\ \text{in.-oz-sec}^2$$

Figure 2-13. Transfer Function Diagram

$$CLR_{major} = \frac{\frac{AK_mK_p}{JN}}{S^2 + \frac{R+AK_mK_T}{J} + \frac{AK_mK_p}{JN}} = \frac{W_o^2}{S^2+2\zeta' W_o S+W_o^2}$$

Substituting values, it is found that

$$W_o = \sqrt{\frac{AK_mK_p}{JN}} = 76.6 \text{ (or fo = 12.2 cps)}$$

and $$\zeta \approx \frac{K_T}{2}\sqrt{\frac{NAK_m}{JK_p}} \approx 1, \text{ critical damping ratio}$$

since $$R \ll AK_mK_T$$

The velocity constant can be estimated as follows:

Full speed at the Risley prism (6000 rpm/118 ≈ 5.3 radian/second) is produced with a motor voltage of 36 vac or an amplifier input of 0.36 vac. Since the tachometer output will be 3.6 vac, then the CT voltage must be 3.6 + 0.36 ≈ 4 vac which corresponds to about 10 degrees = 0.175 radian of error. The K_v is, therefore, 5.3/0.175 or 30 second^{-1}.

The static error can be expected to run about 1 to 2 volts in terms of motor control voltage or about 15 mv at the CT. This requires about a 2 1/4 arc-minute shaft offset.

Another component of static error arises because of in-phase tachometer null voltage but this is not expected to be greater than about 15 mv. Hence a total static error of approximately 4 arc-minutes could be anticipated at each CT shaft.

2.2.4 Measured Results

2.2.4.1 Electrical

The measured results are summarized in Table 2-2. The electrical performance is nominally as expected.

2.2.4.2 Optical

The optical accuracy of the transmit beam offset subsystem was measured with a high precision two-axis autocollimator prior to incorporation into the breadboard. It should be noted that in the breadboard the optical system serves to demagnify, by a factor of 100, the magnitude, M_{PA}, of any angular deviation introduced by this subsystem alone. However, any roll angle, θ_{PA}, that it may introduce about the line of sight is independent of the rest of the optical system.

The precision pair of Risley prisms was designed for a maximum deviation angle of nominally 6 arc-seconds referred to the output of the telescope or 10 arc-minutes for the transmit beam offset subsystem alone.

The goniometers that control each prism element separately were adjusted to produce maximum deviation by the prisms. The third goniometer, which serves to electrically gang the individual servos for roll compensation, was then rotated by 10-degree increments and the resulting magnitude and direction of the deviation angle were measured with the autocollimator. (The goniometers were sufficiently accurate in this case so as not to affect the accuracy of the optical measurements.) The results of one such set of measurements are summarized in Table 2-3.

TABLE 2-2. SUMMARY OF ELECTRICAL MEASUREMENTS

PARAMETER	LOWER* SERVO	UPPER* SERVO	EXPECTED
1) Synchro Scale Factor (volts/degree)	0.32v/1°	0.30v/1°	0.4v/1°
	0.66v/2°	0.64v/2°	0.8v/2°
	1.21v/4°	1.4v/4°	1.6v/4°
Estimated Average** (volts/degree)	0.3 v/°	0.35 v/°	0.4 v/°
2) Stiction Error			
2.1) Maximum Observed Amplifier Input In-phase Error Signal (mv rms)	40	26	15
2.2) CT Shaft Equivalent Angular Error (arc-minutes)	7.5	4.9	2 1/4
3) Tachometer Induced Static Error			
3.1) Maximum Observed Tachometer Null In-phase Output Voltage (mv rms)	12	14	15
3.2) CT Shaft Equivalent Angular Error (arc-minutes)	2.2	2.6	2 1/4
4) Maximum Observed Motor Voltage at Null (volts rms)	3.2	1.9	5
5) 400-cps Amplifier Gain			
5.1) Input Signal Required for 15-volt Output (mv rms)	160	150	150
5.2) Gain (v/v)	94	100	100

* The Lower Servo utilizes test point #1
The Upper Servo utilizes test point #3

** Since the synchro scale factors were less than nominal (0.4 v/°), the amplifier gains were trimmed upwards, after the above measurements, to obtain nominal loop gain characteristics. The servo 33K ohm input resistors were paralleled with 82K ohm (lower servo) and 180K ohm (upper servo) resistors to accomplish the gain increases. The theoretical resistances required were calculated as 79K ohm and 194K ohm, respectively.

TABLE 2-3. SUMMARY OF OPTICAL MEASUREMENTS

Parameter	Measured	Expected	Needed for Synchronous Satellite	Needed for Martian Probe
RMS departure of measured "roll" angle θ_{PA} from "roll" goniometer setting	±9 arc-minutes	±15.3 arc-minutes	± 2 degrees	± 13.5 arc-minutes
Relative RMS deviation of magnitude M_{PA} of deviation angle from mean	± 0.25% of 6 arc-seconds	± 0.7% of 4 arc-seconds	± 3.5% of 4 arc-seconds	±0.4% of 36 arc-seconds

SECTION III

COARSE ACQUISITION SUBSYSTEM

3.1 INTRODUCTION

The coarse acquisition subsystem has the function of detecting a beacon image when it falls within the 1-degree (nominal) coarse acquisition field and of specifying whether it is up, down, left or right of center where the fine guidance field is located. (See, for example, Figure 1-1.) The most direct way of sensing image location is to divide the image plane optically into four distinct sectors for subsequent photoelectric processing. In carrying out this processing, it is desirable that moving parts, such as choppers, be avoided and that a minimum number of detectors be employed. Also, because photocathodes are usually not very uniform spatially, it is desirable to provide condensing optics such as field lenses that fix the distributions of light falling on the detectors.

Based on these considerations, a coarse acquisition was developed and incorporated into the laser telescope breadboard. A description of this work is given in the present section.

The subsystem employs a novel optical element that acts as a combination field splitter and field lens. This element is followed by a four-quadrant multiplier phototube, which functions with the aid of simple switching electronics as four distinct photomultipliers within a single rugged envelope.

This is a new approach and was chosen over the use of fiber optics previously suggested in reference 1* mainly because the new design is able (1) to take advantage of the inherent simplicity and reliability of the recently developed quadrant multiplier phototube (or equivalent detector approaches) and (2) to offer improved light transmission as compared with fiber optics.

3.2 OPTICAL APPROACH

The design approach of the coarse acquisition subsystem relies on the inherent simplicity (once fabricated) of an optical image splitting element, and is illustrated in Figure 3-1. A folding flat brings the image plane of the coarse acquisition field to the position shown and transmits the fine guidance field through a central elliptical aperture. A special field lens is located at the coarse acquisition image plane. It serves to image the entrance pupil of the telescope - in this case, the periphery of the primary mirror - onto the plane where the detector is located. The second surface of the field lens is pyramid-shaped which results in four separate images of the telescope's entrance pupil being formed in the detector plane. Each image corresponds to one quadrant of the coarse acquisition field. A predetection spike filter substrate precedes the field lens where the incident f/15 cone angle is approximately 4 degrees (2-degree semi-angle).

The field splitter/field lens is fabricated from a special glass type that has an index of refraction of nearly 2 (Schott SFS-1). This enables a very short focal length to be achieved without having a steep lens curvature. It also has the advantage that a single antireflection coating of MgF (index of nearly $\sqrt{2}$) results in negligible reflection losses at each air-glass surface.

* Op. Cit., page 1-1.

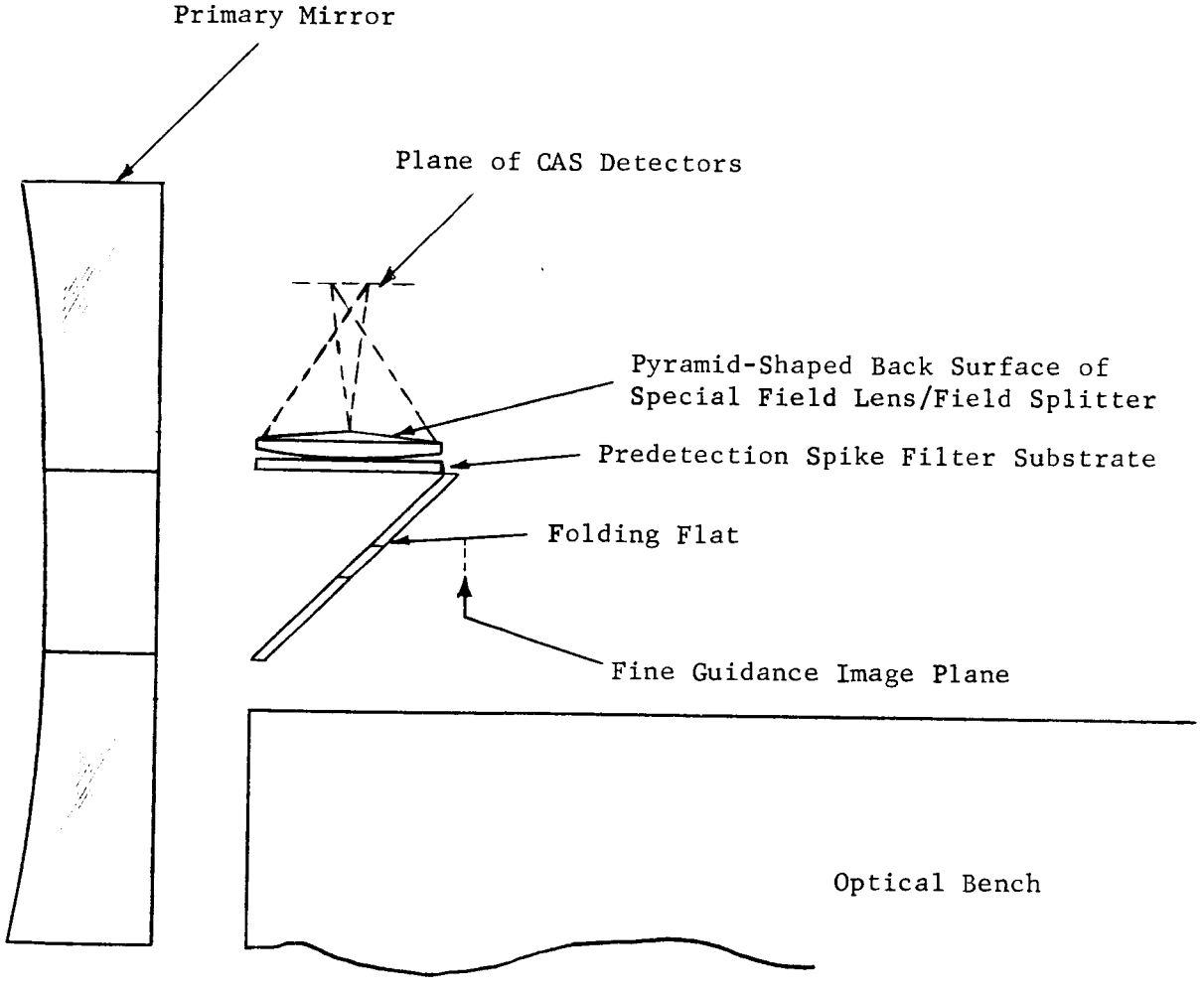

Figure 3-1. Arrangement of Coarse Acquisition Subsystem Optics

A view of the pyramidal surface of the field splitter is shown in Figure 3-2. Figure 3-3 illustrates the formation of four distinct images of a distant photoflood lamp by the field splitter, while Figure 3-4 illustrates the appearance of a single penny viewed through the field splitter.

All optical components of the coarse acquisition subsystem fit into a housing that attaches directly to the main telescope structure. This housing compactly supports the entire subsystem and may be seen in Figure 1-2.

A functional check of the optical components of the coarse acquisition subsystem was carried out and it was determined that the special field splitter functions substantially as expected. It indeed causes the image plane of the coarse 1-degree (nominal) field to be split into four segments. When the beacon image falls anywhere within a given quadrant, a stationary circular patch in the plane of the respective detector quadrant becomes uniformly illuminated.

3.3 DETECTOR APPROACH

The optical design of the coarse acquisition subsystem makes it natural to consider using a quadrant multiplier phototube (QMP), such as EMR type 573-E, as the detector for the subsystem. This is because field splitting is carried out by an optical element preceding the QMP, which eliminates any signal loss that otherwise would be associated with the "dead" regions between the photocathode quadrants. (See, for example, Table 3-2 of Reference 1,* p. 3-21.) Furthermore, as an added refinement, it is possible to combine two such detectors with a beamsplitter in order to have a fully redundant detector configuration.

*Op. Cit., page 1-1.

Figure 3-2. View of Field Splitter in its Cell

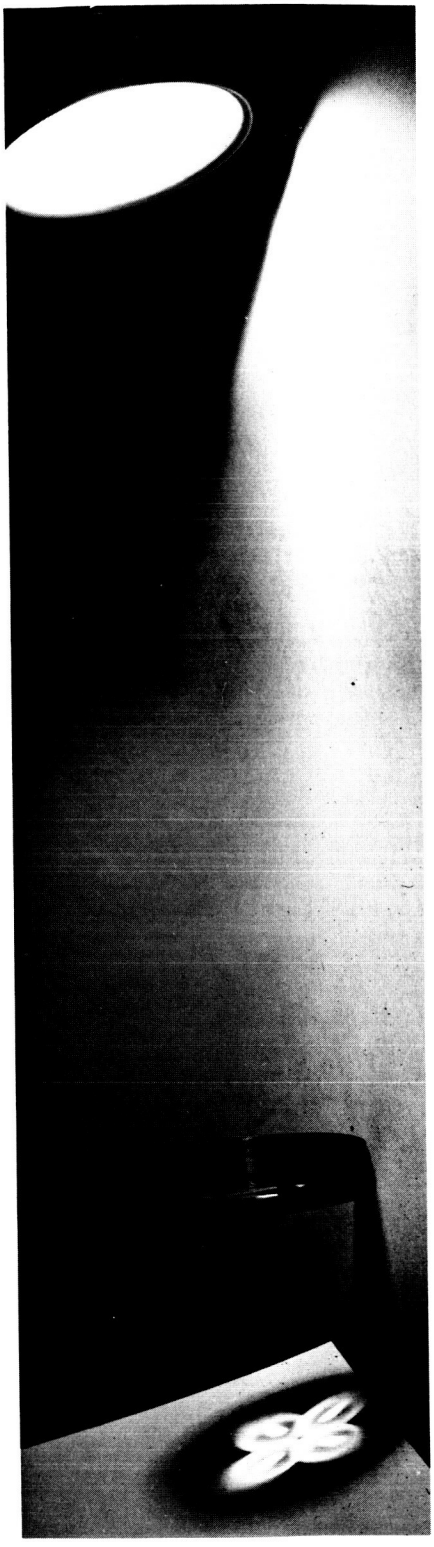

Figure 3-3. Photograph Showing Multiple Image Formation of a Distant Photoflood Lamp by the Field Splitter

Figure 3-4. A Single Penny Viewed Through the Field Splitter

A prototype EMR type 573 E-01-14 quadrant multiplier phototube was loaned to us by the manufacturer for evaluation purposes, and it was successfully incorporated into the breadboard. The characteristics of this tube are summarized in Table 3-1.

TABLE 3-1. MANUFACTURER'S DATA FOR EMR TYPE 573E-01-14 QUADRANT MULTIPLIER PHOTOTUBE SERIAL NO. D-7637

Spectral response	S-20
Average luminous sensitivity	156 microamperes/lumen
Quantum efficiency (%) at 4100Å	Quadrant 1: 19.4 Quadrant 2: 15.6 Quadrant 3: 17.5 Quadrant 4: 20.8
Amplification	10^5 at 1910 volts; dark current 4 x 10^{-11} amperes 10^6 at 2490 volts; dark current 5 x 10^{-10} amperes 10^7 at 3280 volts; dark current 3.7 x 10^{-9} amperes
Leakage between quadrants	$< 10^{-11}$ amperes
Signal ratio from "on" to "off" cathode when light is on "on" cathode (current amplification of 10^6)	Average 60

(Ordinarily, quoted delivery on detectors of this type is about four months after receipt of order and they are expensive. These reasons would have precluded purchase of a QMP for the breadboard experiments. An alternative approach would have been to use a cluster of four small-diameter photomultipliers and to arrange to switch them sequentially. This would have simulated the use of the four-quadrant device at considerable savings in time and funds.)

The quadrant multiplier phototube consists of four electrically independent cathode quadrants followed by a common electrode chain consisting of a bias electrode, a focus electrode, and 14 dynode stages. A given quadrant is "on" when it is at the same potential as the bias electrode. The "off" condition is achieved by biasing a quadrant approximately 20 volts positive with respect to the bias electrode.

Special QMP switching circuitry was developed for the coarse acquisition subsystem, which biases two adjacent quadrants on, and holds the opposite half of the photocathode off. Every quarter cycle, this half-on, half-off photocathode configuration is rotated by 90 degrees. The effect is much as if a semicircular chopping wheel were rotated in front of four separate photomultipliers, each of which senses one quadrant of the coarse acquisition field. It is readily established that, with reference to the chopping cycle, the in-phase and quadrature signals at the output of the detector indicate unambiguously the presence of the beacon in the respective quadrant of the coarse acquisition field.

The schematic of the switching circuitry is shown in Figure 3-5 and provides square-wave control signals to switch the four cathode quadrants sequentially as required. Flip-flop FF-1 changes state upon a trigger input transition from a silicon control switch (SCS) oscillator. The complementary outputs of FF-1 are directly coupled to a pair of flip-flops, FF-2 and FF-3. In order to avoid phase ambiguity, a proper reset is provided between the two flip-flops so that the state of one controls the state of the other. The photographic waveforms of the four outputs are shown in Figure 3-6.

Four transistors with common emitter configuration are connected between each cathode of the multiplier phototube and the bias electrode (ground). The transistors are switched to either the high-impedance cutoff or the low-impedance saturation state by applying square-wave biasing signals to the corresponding bases. The anode current of the SCS with the circuit configuration shown is extremely low when the gate to anode is zero, and it is possible to produce very long duration trigger pulses with small timing capacitors. The time duration of oscillation can be approximated from solving the following equation:

$$V_1 \left\{1 - \exp\ (-t/RC)\right\} + 0.67 \exp\ (-t/RC) = V_1 \left(\frac{R_2}{R_1 + R_2} \right) + 0.67$$

Substituting typical values, V_1 = 3.6 volts, R_1 = 18 K, and R_2 = 10 K, we obtain t = 0.58 RC.

The actual switching electronics for the QMP are illustrated full scale in Figure 3-7. Three microcircuit flip-flops are utilized, and are situated as shown in the lower left-hand area of the circuit board. Front

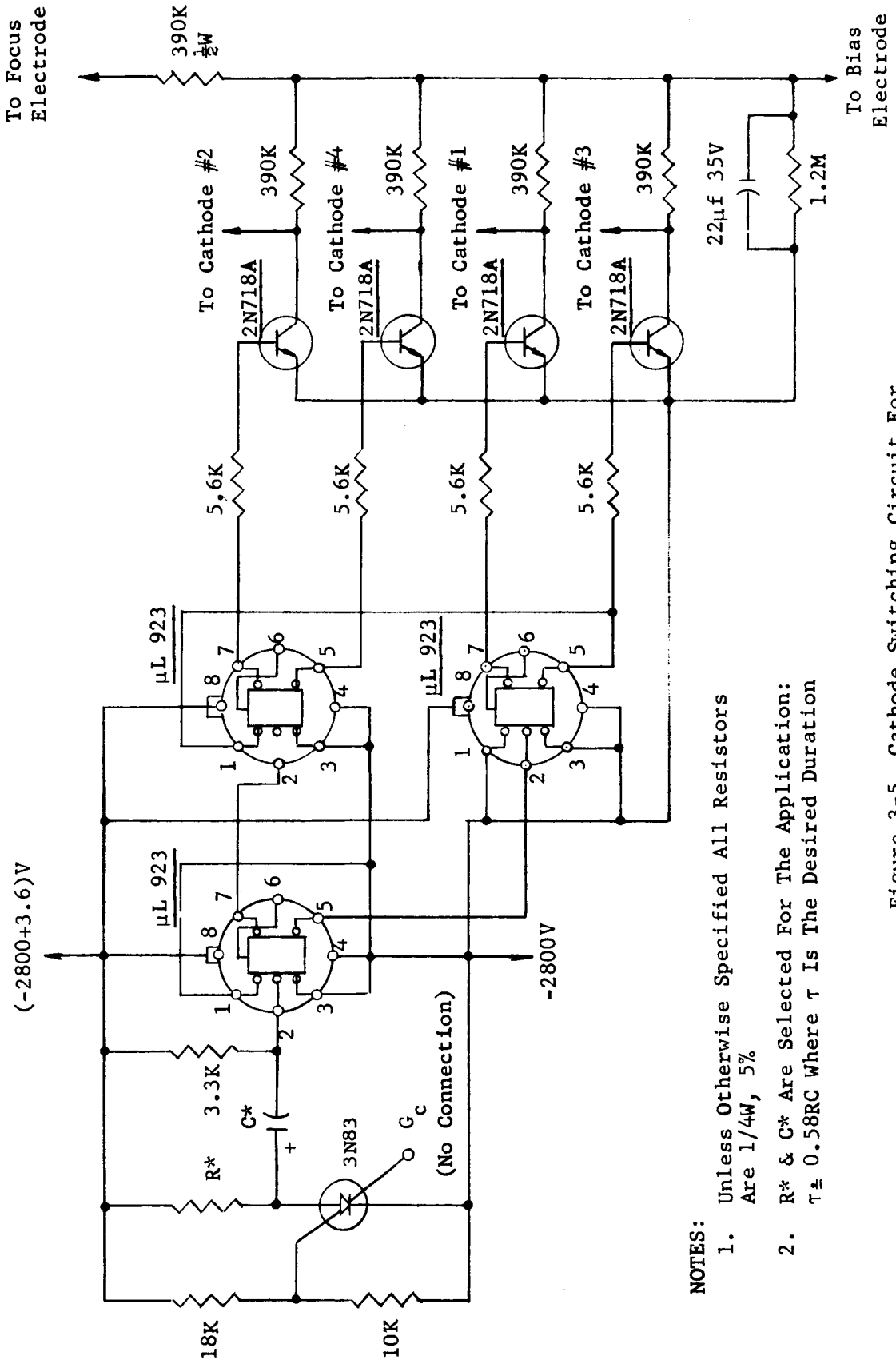

NOTES:

1. Unless Otherwise Specified All Resistors Are 1/4W, 5%
2. R* & C* Are Selected For The Application: $\tau \pm 0.58RC$ Where τ Is The Desired Duration

Figure 3-5. Cathode Switching Circuit For Quadrant Multiplier Phototube

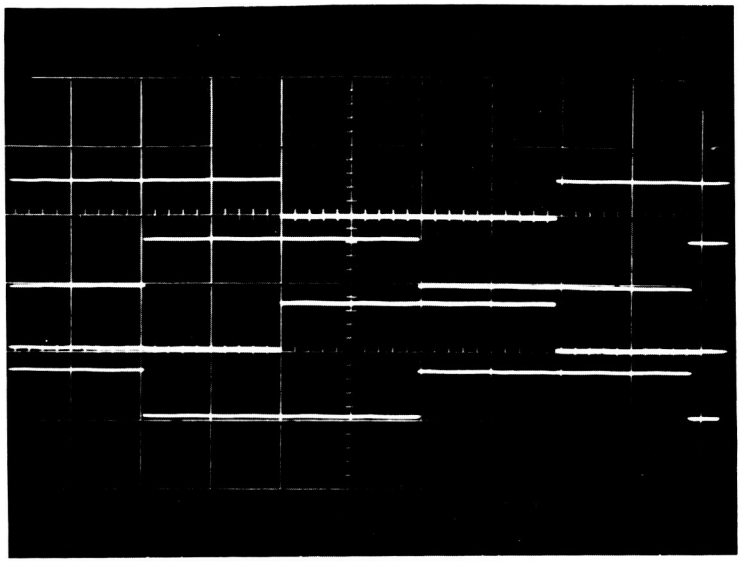

Figure 3-6. Comparison of Four Control Waveforms at Ⓐ, Ⓑ, Ⓐ̄, and Ⓑ̄, from Top to Bottom

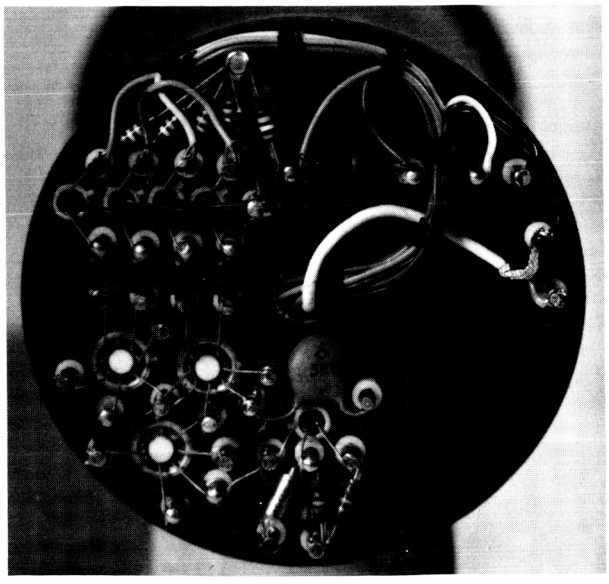

Figure 3-7. Full Scale Photograph of the Switching Electronics for the Quadrant Multiplier Phototube

and rear views of the QMP with the electronics board are shown in Figures 3-8 and 3-9, respectively. The complete detector assembly is illustrated in Figure 3-10.

3.4 RESULTS

3.4.1 QMP Performance

The coarse acquisition subsystem was incorporated into the breadboard which, by means of a test collimator and a movable light source, was arranged to receive simulated beacon light over various field angles. With beacon light present on one of the quadrants of the QMP, it was found that the ratio of the "on" signal to the "off" signal at the anode of the QMP was typically 14/1, without taking any special precautions to prevent scattered light from reaching the other quadrants. According to data provided by EMR, higher values can readily be achieved if better isolation is necessary.

Figure 3-11 illustrates one cycle of the QMP anode signal for beacon light (chopped at 150 Hz) entering the laser telescope and falling only on quadrant designated number 4. Similarly, Figure 3-12 illustrates beacon light falling only on quadrant 1. Figure 3-13 illustrates an intermediate situation resulting from the beacon image being incident on the intersection of two planes of the optical field splitter and falling both on quadrants 4 and 1.

The switching rate was varied from approximately 10 Hz to 1 Hz. It was found that, with square switching pulses, two of the four quadrants had a slow turn-on time, the slowest being on the order of 0.1 second. Presumably, this unexpected characteristic was due to a poor cathode connection of unusually

Figure 3-8. Front View of the Quadrant Multiplier Phototube

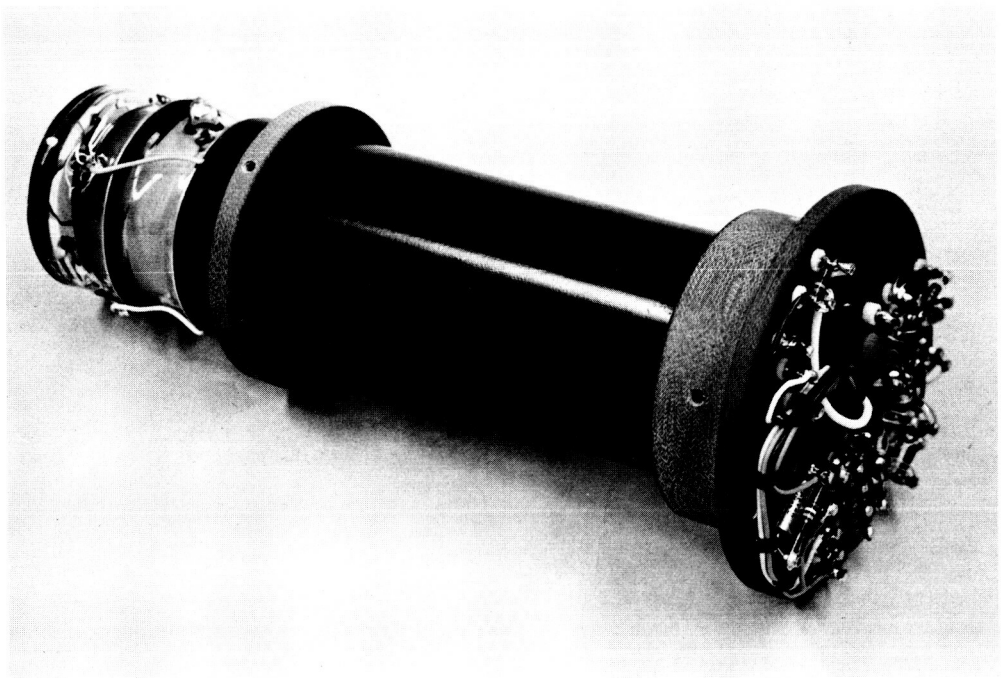

Figure 3-9. Rear View of the Quadrant Multiplier Phototube

Figure 3-10. Photograph of Complete Coarse Acquisition Detector Assembly

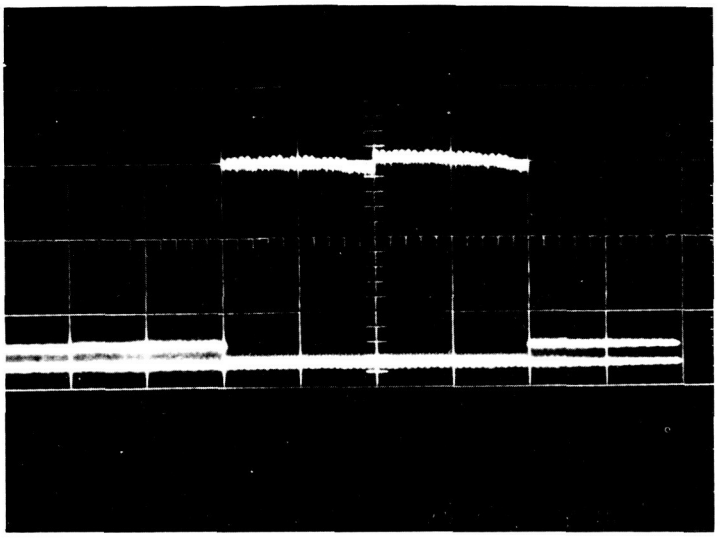

Figure 3-11. QMP Anode Signal for Beacon Light Entering the Laser Telescope and Falling Only on Quadrant 4. Vertical scale 2.4v/cm; horizontal scale 0.08 sec/cm. Beacon chopped at 150Hz. The intermediate change in signal level is evidently the result of having different quadrant pairs "on."

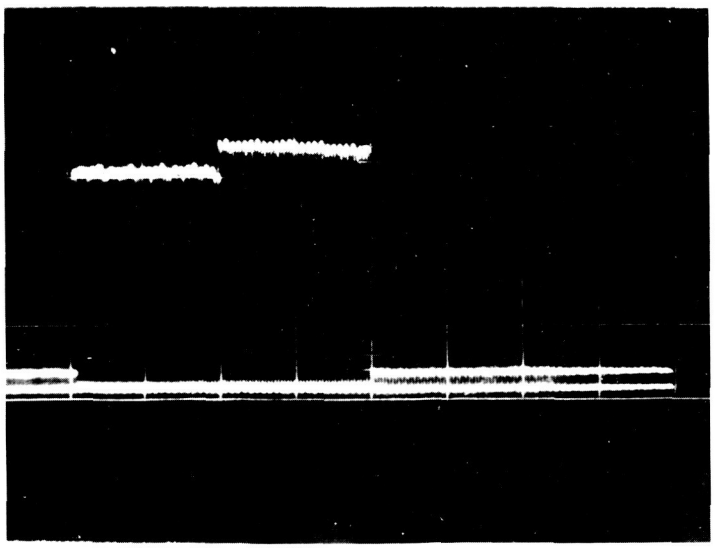

Figure 3-12. QMP Anode Signal for Beacon Light Entering the Laser Telescope and Falling only on Quadrant 1. Conditions otherwise as in Figure 3-11.

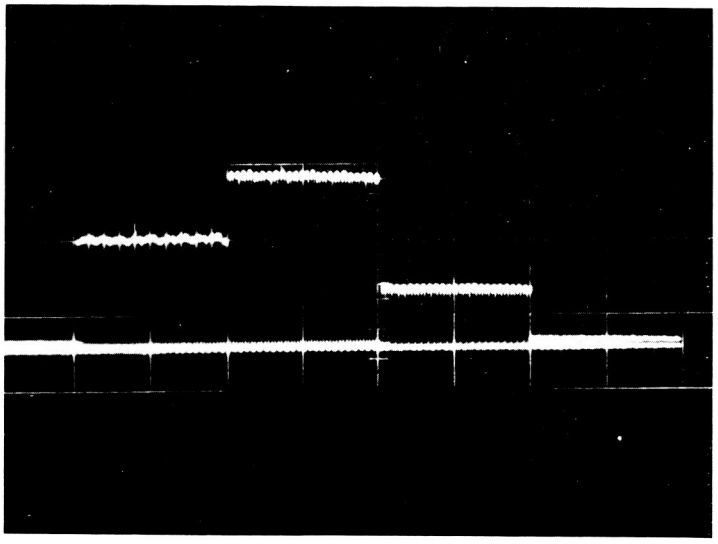

Figure 3-13. QMP Anode Signal for Beacon Light Split Unequally Between Quadrants 4 and 1. Conditions of Photograph as in Figures 3-11 and 3-12.

high resistance. According to EMR, who provided this prototype tube for evaluation purposes, cathode turn-on time is not ordinarily a problem. Indeed, other QMP's of this type have been used with switching rates exceeding 1 KHz.

In other respects, such as photocathode sensitivity, photocathode uniformity, and anode dark current, the EMR device is comparable to conventional high quality photomultipliers having an S-20 response. However, its use in the coarse acquisition subsystem is characterized as follows: the QMP acts as four photomultiplier tubes in a single envelope, which makes for a compact package; and, because chopping is carried out electronically, no moving parts are required in the subsystem.

3.4.2 Dependence of Acquisition and Tracking Signals on Beacon Angle

The outputs of the coarse acquisition and fine guidance subsystems were measured as a function of beacon position in the field of view of the laser telescope breadboard. The test setup was as shown in Figure 3-14, with the microscope light source assembly mounted on a precision two-axis stage shown in Figure 3-15. This arrangement permitted moving the simulated beacon source to various accurately located positions covering more than the nominal 1-degree field of view of the breadboard.

The outputs of the coarse acquisition and fine guidance subsystems are shown in Figure 3-16 as a function of the direction of the beacon. The vertical scale is normalized with respect to the maximum signal from each subsystem, respectively. The horizontal scale denotes the position of the beacon relative to the nominal axis of the laser telescope. This plot shows

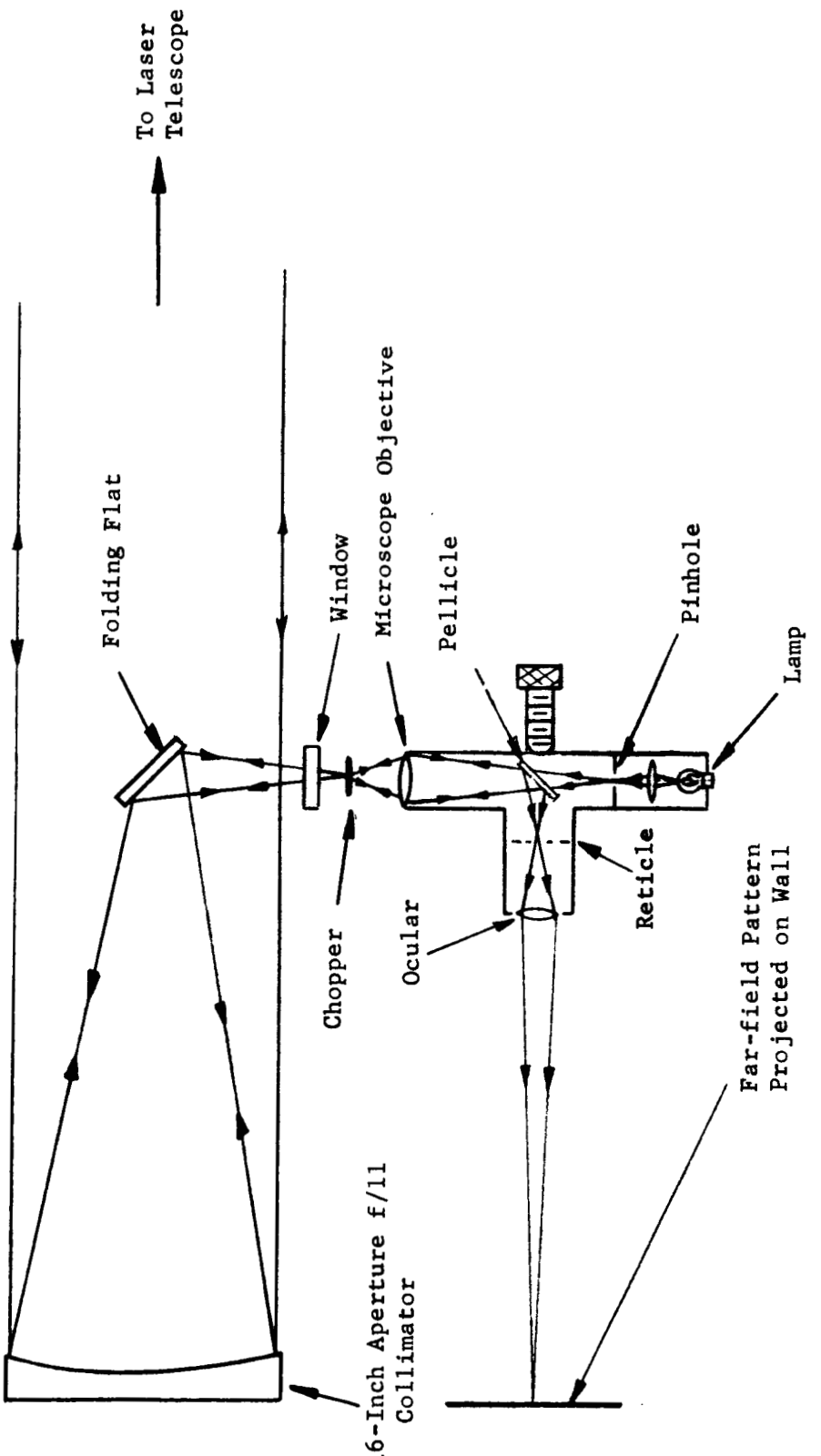

Figure 3-14. Layout of Test Setup for Acquisition and Track Experiments

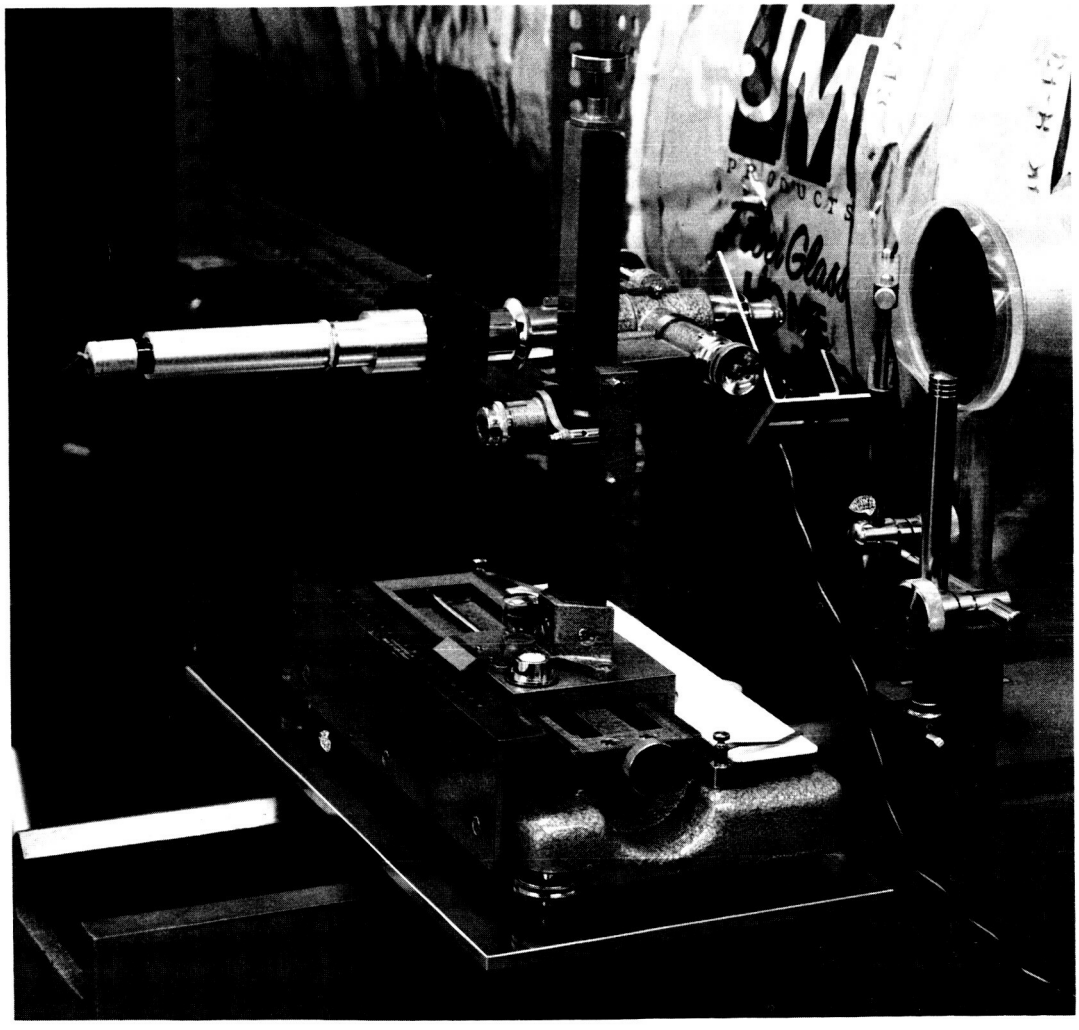

Figure 3-15. Photograph of the Microscope Light Source Assembly Mounted on a Precision Two-axis Stage

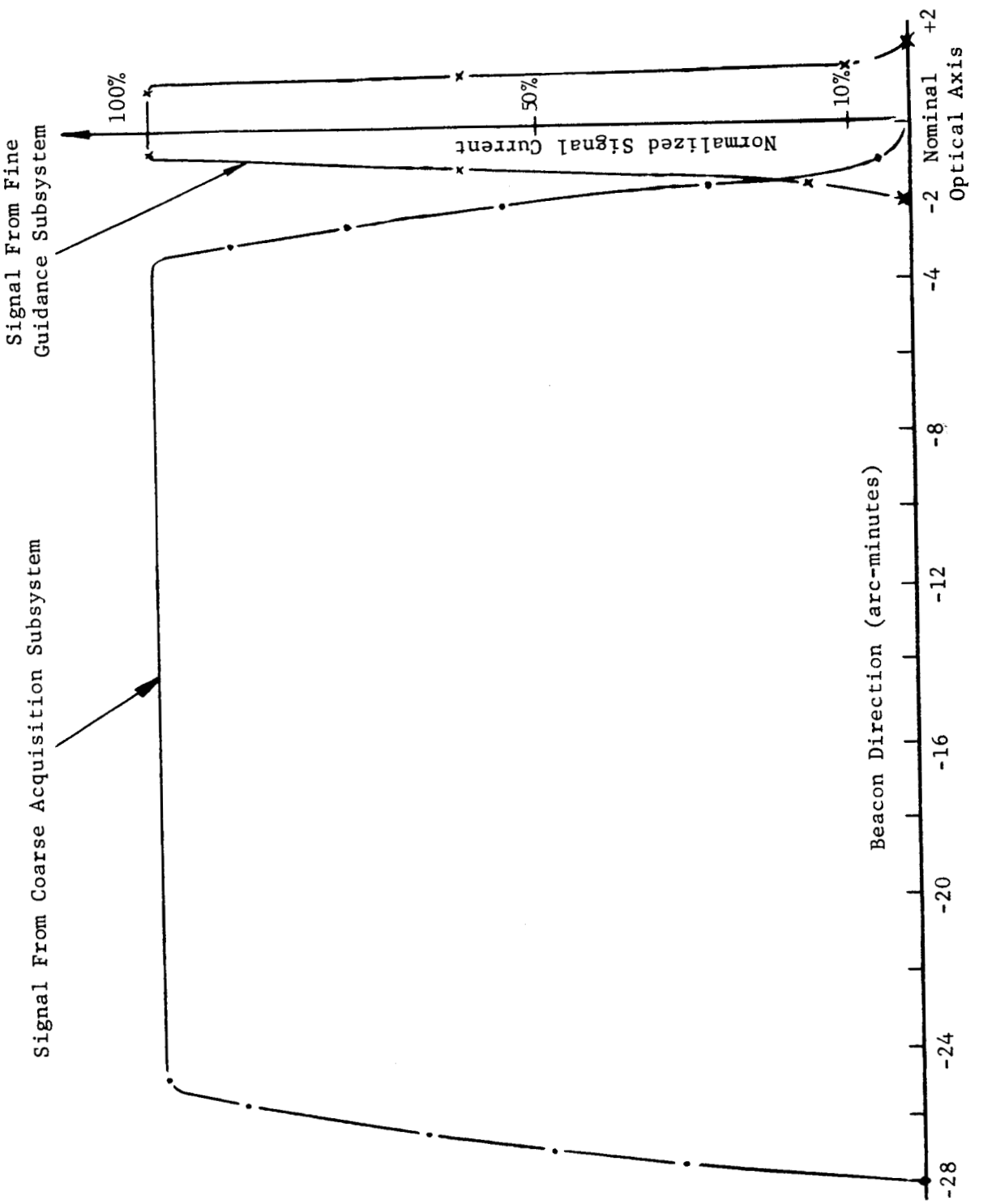

Figure 3-16. Plot of Coarse Acquisition and Fine Guidance Signals as a Function of Beacon Direction

that the fine guidance field is completely unvignetted over somewhat more than the design value of 2 arc-minutes.

Between the regions of coarse and fine field detector maxima, lies a small intermediate annulus where the optical system fails to throw all of the beacon light into one region or the other. The diameter of the perforation in the folding flat (Figure 3-1) is evidently slightly too large, and may be reduced to increase the efficiency in this annulus.

The signal from the coarse acquisition subsystem detector shows that beacon light is essentially unvignetted by the laser telescope between the semi-field angles of 26.6 arc-minutes and 2 arc-minutes.

The diameter of the clear aperture of the coarse acquisition optical assembly is 4 inches. For the 240-inch effective focal length of the telescope, this corresponds to a maximum semi-field-angle of 28.6 arc-minutes with some vignetting expected at the edge of the field. The optical performance of the coarse acquisition subsystem is, therefore, nominally as expected.

SECTION IV

ACQUISITION AND TRACK SIMULATION

With continuing development of techniques for deep-space optical communications, it has been increasingly important to study ways of simulating beacon acquisition and precision beam pointing operations under conditions that realistically simulate space operation. Experiments were, therefore, conducted with the laser telescope to demonstrate visually the essentials of these operations and to point the way for subsequent, more detailed simulation experiments.

The breadboard was set up with the collimator and precision beacon source previously illustrated in Figure 3-14. This arrangement displays a greatly magnified image of the far-field pattern of the transmitted He-Ne laser beam. Visual comparison of this image, when the system is tracking the beacon and when it is not, gives a direct evaluation of the tracking scheme. Typical room vibrations and pressure applied to the laser telescope optical bench were seen to cause fluctuations of up to several arc-seconds in the telescope's line of sight unless the transfer lens servo was switched to the track mode. Initially, the setup was shown to work without taking precautions to eliminate excessive vibration and air turbulence, but the imagery was unsatisfactory. Steps were therefore taken to improve the optical alignment of the system and to isolate the system from the major disturbances. Also, in these early experiments, a cathode ray tube (CRT) was substituted for the tungsten source illustrated in Figure 3-14. It was shown that the laser telescope

was capable of tracking a moving spot on the face of the CRT. This established that future simulation experiments can be carried out with a suitably designed flying spot scanner as the simulated beacon source.

The next step in the simulation experiments was to lengthen the laboratory housing the Laser/Optics Techniques project by more than 8 feet to permit greater spacing between the laser telescope and the test collimator. At the same time, new vibration-isolated support stands were constructed for the collimator and its associated diagonal mirror and light source optics. The complete system was then carefully realigned. It was again possible to project a greatly magnified diffraction pattern of the laser telescope directly on the wall by means of the arrangement shown in Figure 3-14. During brief periods, when the air in the laboratory was still, the pattern resembled a classical Airy pattern. The position of this pattern was observed to be stabilized within a fraction of the diameter of the central ring when the system was switched to the beacon track mode. However, air turbulence prevented diffraction-limited imagery except on a transient basis.

To improve this situation (which is nevertheless capable of demonstrating fractional arc-second tracking accuracies), we arranged to completely enclose and seal the wide aperture optical paths by means of aluminum housings and ducts. These enclosures were heavily insulated on the outside, and were intended to act as an isothermal enclosure of good interior heat conductivity to stabilize the air in the light paths. Although somewhat astigmatic, possibly because of stratification of air in the enclosure, it was observed that the shape of the image was now stable. To compensate for the astigmatism, a plane-parallel window was inserted in the optical path between the microscope

and the enclosure window and was tilted until a symmetrical image resulted. With the imagery thus corrected, the diffraction pattern then resembled a classical Airy pattern and its shape was stable for long periods of time.

Tracking and pointing functions of the breadboard were demonstrated with the aid of a globe of the earth mounted adjacent to the wall on which the image was projected. The geometry of the setup was such that the diameters of the globe and the projected image were scaled to the geometry that would result from an earth-spacecraft range of 10^8 miles (i.e., the globe subtended an angle of approximately 15 arc-seconds as seen by the laser telescope). The position of the simulated beacon was made to correspond with a given point on the globe. The demonstration consisted of, first, mispointing the laser telescope by some tens of seconds of arc so that the projected image missed the globe by several "earth" diameters. Then, the breadboard was switched to track. The image would immediately acquire and track the beacon. As a result, the image appeared to swing to an appropriate spot on the globe where it would stay locked to within a fraction of its diameter, even in the presence of pointing disturbances introduced into the laser telescope.

Figure 4-1 shows a 30-second time-exposure photograph of the projected image on the globe. The low light levels in this experiment were not completely satisfactory for taking photographs in this way. Although the essential features of the image may be seen in Figure 4-1, the actual visual appearance of a classical Airy pattern, the position of which is stabilized in practice to within a fraction of its diameter, is not conveyed by this still photograph.

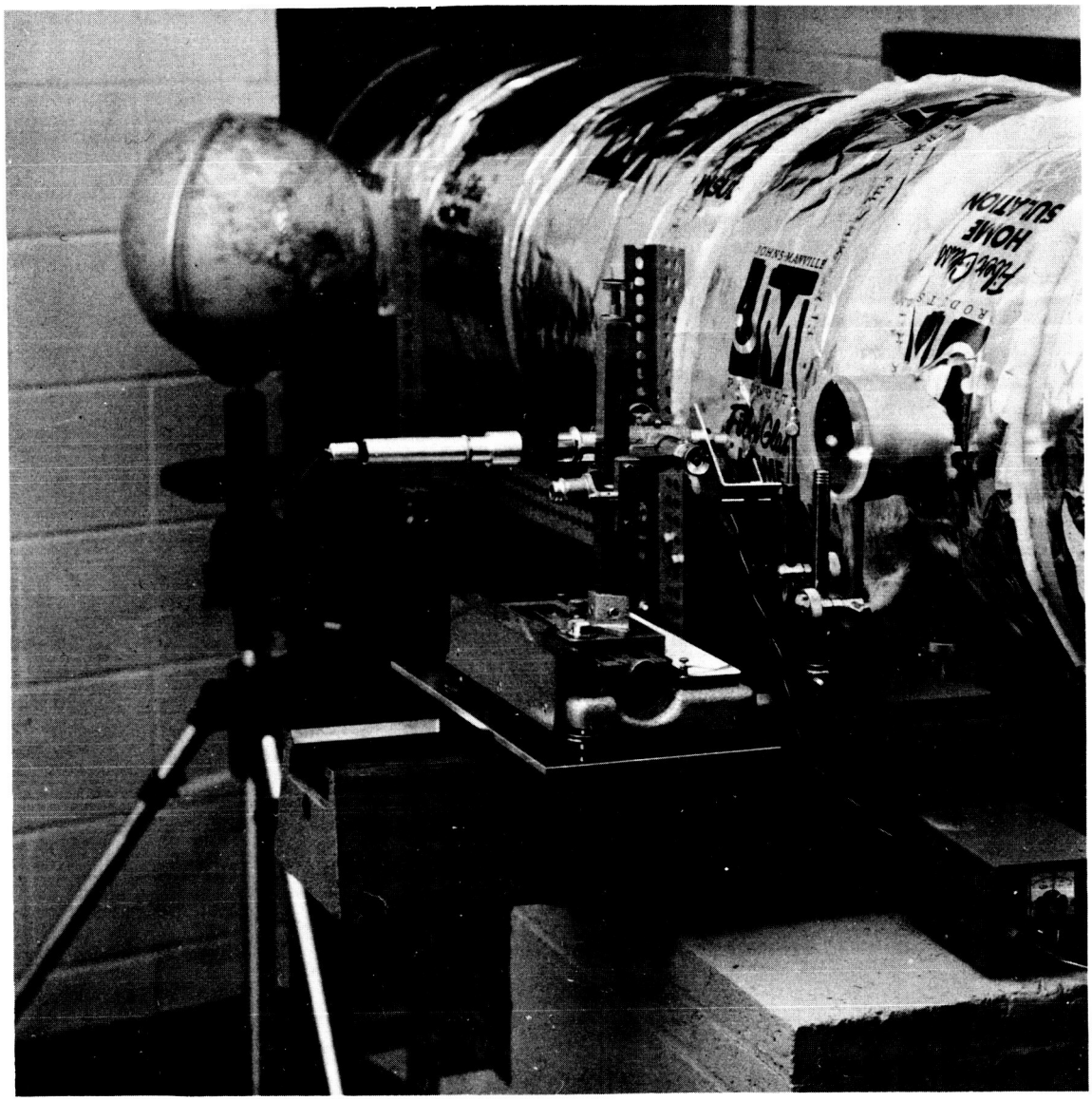

Figure 4-1. The Far-field (Airy) Pattern of the Laser Telescope Projected on a Globe of the Earth as if From a Distance of 10^8 Miles Away

In addition, the functions of the transmit beam offset subsystem could be readily demonstrated. While the system was tracking, the projected image was repositioned remotely away from the line of sight so as to make it fall with diffraction-limited precision on various points on the globe. Compensation for vehicle roll was then illustrated by causing the image to rotate about the zero offset line of sight.

SECTION V

DISCUSSION

Exceptionally narrow beamwidths are attainable with laser sources and diffraction-limited optics. This fact accounts for the great promise of laser systems to complement conventional microwave systems and achieve wide bandwidth communications across extreme distances. It also accounts for the major difficulties commonly thought to lie between promise and practice. After all, narrow beamwidths will hit their mark only with correspondingly accurate techniques for target acquisition and tracking and for laser beam pointing.

A previous report* describes the development of some key hardware needed to overcome these difficulties. In the course of this earlier work, a start was made on the breadboarding of all the essential parts of the deep-space optical communications system.

The breadboard employs a 16-inch aperture telescope and is capable of tracking a laser beacon and pointing a transmitted beam to within a fraction of its fundamental 0.4-arc-second diffraction spread. An optical duplex system configuration is used. Isolation of more than 115 db between transmit and receive channels is achieved by means of special dielectric multilayer techniques. A servo-controlled transfer lens is incorporated in a way that permits diffraction-limited tracking of a distant beacon over a 2-arc-minute diameter fine guidance field.

*Op. Cit., Page 1-1.

This earlier work was supplemented during the period from 29 April 1966 to 31 December 1966, by the development of additional key hardware which is now incorporated into the breadboard to form a more nearly complete system. The present report describes this recent work. In particular, two new subsystems are described, a coarse acquisition subsystem (for wide-field beacon acquisition) and a transmit beam offset subsystem (for transmitter "point ahead" and spacecraft roll compensation).

In addition preliminary experiments were recently carried out with the breadboard to demonstrate visually its fractional arc-second beacon tracking and beam pointing accuracy under conditions that simulate those under which the system would operate in deep space. As discussed in Section IV, the far-field (Airy) pattern of the laser telescope was projected on a simulated earth as if from a distance of approximately 10^8 miles away. The laser telescope was arranged to track a source that simulates a beacon on the earth's surface. It was determined from visual observations that the Airy pattern on the globe was stationary to within a fraction of the diameter of its central core, which corresponds to an angular accuracy on the order of 1/10 arc-second. This tracking accuracy is maintained by the transfer-lens servo in the presence of manually introduced pointing errors (within the servo bandwidth) that would amount to tens of arc-seconds open loop.